

Contemporaneous Observations of $H\alpha$ Luminosities and Photometric Amplitudes for M Dwarfs

AYLIN GARCÍA SOTO,¹ ELISABETH R. NEWTON,¹ STEPHANIE T. DOUGLAS,² ABIGAIL BURROWS,¹ AND
AURORA Y. KESSELI³

¹*Department of Physics and Astronomy, Dartmouth College, Hanover NH 03755, USA*

²*Department of Physics, Lafayette College, Easton PA 18042, USA*

³*Infrared Processing and Analysis Center, Caltech, Pasadena CA 91125, USA*

ABSTRACT

While many M dwarfs are known to have strong magnetic fields and high levels of magnetic activity, we are still unsure about the properties of their starspots and the origin of their magnetic dynamos. Both starspots and chromospheric heating are generated by the surface magnetic field; they produce photometric variability and $H\alpha$ emission, respectively. Connecting brightness variations to magnetic activity therefore provides a means to examine M dwarf magnetism. We survey 30 M dwarfs previously identified as fast rotating stars ($P_{rot} < 10$ days). We present time-series optical photometry from the Transiting Exoplanet Survey Satellite (TESS) and contemporaneous optical spectra obtained using the Ohio State Multi-Object Spectrograph (OSMOS) on the 2.4m Hiltner telescope at MDM Observatory in Arizona. We measure rotation periods and photometric amplitudes from TESS light curves using Gaussian Processes. From the OSMOS spectra, we calculate the equivalent width of $H\alpha$, and $L_{H\alpha}/L_{bol}$. We find a weak positive correlation between $H\alpha$ luminosity and the semi-amplitude, R_{var} ($p = 0.005^{+0.075}_{-0.005}$). We also observe short-term variability (between 20-45 minutes) in $H\alpha$ equivalent widths and possible enhancement from flares consistent to recent literature.

Keywords: stars: activity — stars: low-mass — stars: rotation

1. INTRODUCTION

M dwarfs make up $\sim 70\%$ of stars in our Galaxy (Henry et al. 2006). Due to their smaller sizes, they produce deeper exoplanet transits and larger radial velocity amplitudes. Thus, they present an easier way to find Earth-size planets compared to FGK stars. However, M dwarfs also pose a problem because they are very magnetically active stars. Active regions on the stellar surface can produce large-amplitude radial velocity signals, masking or masquerading as planets (e.g., Boisse et al. 2011; Haywood et al. 2014; Newton et al. 2016a; Robertson et al. 2020). They also can produce residual features in transmission spectroscopy, masking or masquerading as planetary spectral features, especially water (e.g., Pont et al. 2008; Rackham et al. 2018; Zhang et al. 2018; Wakeford et al. 2019). An in-depth understanding of magnetic activity in M dwarfs—starspots, activity properties, and magnetic dynamos—will support exoplanet research in the decades to come.

Starspots on M dwarfs are assumed to form the same way as sunspots, with dark regions resulting from magnetic field lines rising to the stellar surface. In the Sun, the origin of the magnetic field is thought to be the $\alpha\Omega$

dynamo, where differential rotation and the tachocline, the boundary between the radiative zone and the convective zone, play an important role (Parker 1955; Charbonneau 2010; Cameron et al. 2017). The properties of starspots are therefore an important observational signature of the magnetic dynamo (Berdyugina 2005).

Strong, large scale magnetic fields of M dwarfs have been detected using Zeeman broadening (Robinson 1980; Saar 1988; Valenti et al. 1995) and Zeeman Doppler Imaging (Donati et al. 2008; Morin et al. 2010). However, M dwarfs of masses less than $0.35 M_{\odot}$ are fully convective; they lack a radiative zone and consequently a tachocline (Chabrier & Baraffe 1997). In these stars, $\alpha\Omega$ is likely not the underlying dynamo generating the observed large-scale fields, and it is reasonable to expect different magnetic properties on M dwarfs compared to solar-type stars.

The dynamo and magnetic fields can also be studied through the relationship between rotation period and activity indicators such as chromospheric emission (particularly Ca II H&K and $H\alpha$) and coronal (X-ray) emission. Chromospheric and coronal heating and the resulting emission is thought to reflect the underlying

magnetic dynamo mechanism (Parker 1955; Kim & Demarque 1996).

Those magnetic field proxies are plotted against the Rossby number, the ratio of rotation period to convective overturn time. These relations show two regimes. In the unsaturated regime, activity increases with decreasing period or Rossby number. In the saturated regime, most studies show a plateau inactivity for rapid rotators, at a critical Rossby number $\lesssim 0.1$ (e.g., Reiners et al. 2009). This is seen in Ca II H&K (e.g., Vaughan 1980; Middelkoop 1981; Browning et al. 2010), $H\alpha$ (e.g., Mekkaden 1985; Delfosse et al. 1998; Mohanty & Basri 2003; Reiners et al. 2012; Douglas et al. 2014; Newton et al. 2017; Núñez et al. 2017), X-ray (e.g., Wright et al. 2011; Núñez et al. 2017; Wright et al. 2018; Magaúda et al. 2020), magnetic field strength (Donati et al. 2008; Reiners et al. 2009; Vidotto et al. 2014; Shulyak et al. 2017, 2019; Reiners et al. 2022, e.g.,) and flares (e.g., Davenport 2016; Medina et al. 2020, 2022b). However, others studies show a weak correlation between the Rossby number and activity index in the saturated regime (e.g., Mamajek & Hillenbrand 2008; Reiners et al. 2014; Lehtinen et al. 2021; Magaúda et al. 2020).

The rotation-activity relations show scatter that appears to be intrinsic (Newton et al. 2017; Boudreaux et al. 2022). Newton et al. (2017) noted a relationship between photometric variability amplitude, which derives from starspot-related modulations, and the $H\alpha$ emission line strength, measured relative to the bolometric luminosity, $L_{H\alpha}/L_{bol}$. They find a positive correlation between semi-amplitude and $L_{H\alpha}/L_{bol}$, and concluded that non-sinusoidal rotational variability and spot evolution were likely impacting the results by creating intrinsic scatter.

This paper explores both potential sources of scatter in photometric amplitude, R_{var} and $L_{H\alpha}/L_{bol}$. We address non-sinusoidal rotation by using uniformly-obtained, high S/N light curves and measuring amplitude non-parametrically. We address spot evolution through the use of contemporaneous photometric and spectroscopic observations. To do this, we use photometry from Transiting Exoplanet Survey Satellite (TESS; Ricker et al. 2015) and new spectroscopic data from the Hiltner Telescope 2.4m Ohio State Multi-Object Spectrograph (OSMOS; Martini et al. 2011).

In §2 we present our M dwarf sample and stellar parameters §2.3, in §3 the instruments that we use, in §4 we explain the process of removing stellar flares, the analysis of the photometric and spectroscopic data, and the computation of stellar parameters. In §5 and §6 we compare our results with Newton et al. (2017) and lastly, conclude in §7.

2. SAMPLE

2.1. Northern Hemisphere M dwarfs with rotation and $v \sin i$ Measurements

We cross-match nearby M dwarfs from the MEarth Project (Newton et al. 2016b) with known rotation periods against catalogs containing $v \sin i$ measurements for M dwarfs. We consider three $v \sin i$ catalogs that have large samples of nearby, mid- and late-type M dwarfs ($M < 0.5M_{\odot}$) and which reliably distinguish between detections and non-detections. We then select stars in the Northern Hemisphere with $V < 17.5$ and rotational periods $P_{rot} < 13$ days (corresponding to half of a TESS sector) from the following catalogs:

- Fouqué et al. (2018) presents high resolution spectra of 440 M dwarfs (M0V-M6.5V) taken with the Échelle SpectroPolarimetric Device for the Observation of Stars (Manset & Donati 2003) at Canada-France-Hawaii 3.6m Telescope. This catalog provides $v \sin i$ measurements for 5/30 M dwarfs in our final sample.
- Reiners et al. (2018) analyze high resolution spectra of 324 M dwarfs (M0V-M9V) using the Calar Alto high-Resolution search for M dwarfs with Exoearths with Near-infrared and optical Échelle Spectrographs (Quirrenbach et al. 2012) on the 3.5m telescope at the Calar Alto Observatory. FThis catalog provides $v \sin i$ measurements for 9/30 M dwarfs in our final sample.
- Kesseli et al. (2018) reports the $v \sin i$ of 88 rapidly rotating M dwarfs (M3V-M6V) with spectra taken from the Immersion GRating INfrared Spectrograph (Park et al. 2014) on the Discovery Channel 4.3m Telescope and at the Harlan J. Smith 2.7m Telescope, as well as the iSHELL Échelle spectrograph (Rayner et al. 2016) on NASA’s 3.0m Infrared Telescope Facility. This paper specifically targets M dwarfs from the MEarth Project and so provides significant overlap with our list of rotating M dwarfs. This catalog provides $v \sin i$ measurements for 16/30 M dwarfs in our final sample.

The merged catalog amounts to 133 stars that meet our brightness and P_{rot} limits. Further cuts, as discussed below, reduce our target list to 30 stars.

2.2. Identifying Unresolved Binaries

Initial vetting for unresolved multiple systems was done in Newton et al. (2017) and the three $v \sin i$ catalogs. We further query objects in our sample using the *Gaia* DR2 and DR3 catalog (Gaia Collaboration et al.

2016, 2018, 2022) for the Re-normalized Unit Weight Error (RUWE). RUWE is a chi-square metric of fitting models to single stars, which is intended to remove the dependency of color and magnitude of the *Gaia* Unit Weight Error (Lindgren 2018; Lindgren et al. 2021). Large astrometric errors can indicate binarity, with $\text{RUWE} \gtrsim 1.2$ often used to identify likely binaries (Rizzuto et al. 2018; Bryson et al. 2021). M dwarfs have a significantly lower binary fraction (30%) than higher mass stars (Cortés-Contreras et al. 2017; Winters et al. 2019), yet we find a large fraction of our sample have $\text{RUWE} > 1.2$.

Winters et al. (2021) find that the stars independently identified as binaries have large values of astrometric excess noise, distinct from the single star population. As discussed in §3.3 of that work and references therein, the majority of their sample are assessed for binarity using high-contrast imaging and/or high-resolution spectroscopy. Unsurprisingly, we find that RUWE is also effective at distinguishing the known binaries. However, the median RUWE for likely single, mid-to-late M dwarfs is $\text{RUWE} = 1.2$, with the distribution extending to $\text{RUWE} = 2.1$. 5% of the likely single stars have $\text{RUWE} > 1.6$, while none have $\text{RUWE} < 0.8$. Thus, a different cut-off is needed to identify likely binaries in our sample. We evaluate the RUWE distribution for nearby, mid-to-late M dwarfs in the 15 pc volume-complete sample from Winters et al. (2021).

We fit a Gaussian to the distribution of RUWE for the M dwarfs from Winters et al. (2021) expected to be single stars. Since the RUWE distribution is slightly skewed towards $\text{RUWE} > 1.2$, we only fit the half of the sample at $\text{RUWE} < 1.2$. The standard deviation (σ_{std}) of the fitted Gaussian is 0.13. We adopt $3\sigma_{std}$, or $\text{RUWE} = 1.6$ as the cut-off to identify likely binaries.

We additionally check SIMBAD for references flagging the stars in our sample as binaries. For the stars with $\text{RUWE} > 1.6$, we find the majority of stars were independently identified as binaries. We also manually remove 11 stars with $\text{RUWE} < 1.6$ that have previously been flagged as close binaries. We retain three known binaries which are either more widely separated (> 2170 AU which is resolvable in *Gaia*) or with a dim $V > 17.5$ companion, since we would not expect these companions to affect our results for the primary.

Lastly, we look at the TESS contamination ratios for these stars. This ratio is the fractional contribution of

nearby stars divided by the flux of the target determined in Stassun et al. (2018). For this study, we limit the contamination ratio to $< 20\%$. To determine corrected flux from the primary star or a target, we follow the logic of equation 1 in Rampalli et al. (2019) and substitute the dilution term (neighboring flux over total flux) with the contamination ratio¹. We find that for a neighboring star varying by 5%, its contribution to the light curve is 0.83%. While the flux contribution decreases for dimmer neighboring stars. For example, a neighboring star 2 magnitudes dimmer will only contribute 0.13%.

Our final sample comprises 30 M dwarfs that are well-separated from nearby stars in TESS: 27 M dwarfs that are likely single, 2 binaries with dim companions and 1 wide binary (Table 1).

2.3. Stellar Parameters

2.3.1. Stellar Radii

There are multiple methods to calculate stellar radii: long baseline optical interferometry, analysis the orbit of low mass eclipsing binaries, or comparing spectra to stellar models. However the latter has been shown to underestimate the radius by around 4%. (e.g., Kraus et al. 2011; Feiden & Chaboyer 2012; Spada et al. 2013; Morrell & Naylor 2019). This is thought to be a result of magnetic activity which can inflate active stars relative to inactive stars. Mann et al. (2015, equation 4) derive an empirical relationship between absolute K magnitude (M_K) and the radius based on stars with interferometric radii:

$$R_* = 1.9515 - 0.3520M_K + 0.01680M_K^2 \quad (1)$$

where R_* is the stellar radius in R_\odot and M_K is absolute K magnitude. We use apparent K magnitude from the Two-Micron All-Sky Survey (2MASS; Skrutskie et al. 2006) and parallaxes from *Gaia* DR2 and DR3 catalog (Gaia Collaboration et al. 2016, 2018, 2022) to calculate M_K and then R_* . We use Monte Carlo methods to propagate parallax errors through the calculation, which we add in quadrature with the rms scatter from the empirical relation: 2.89%. The parallax errors (3 – 4%) dominate the final errors on stellar radius. We show the radii measurements in Table 1

¹ A similar logic was applied to transit depths (e.g., Cooke et al. 2018)

Table 1. Parameters for some M dwarfs in Our Sample

TID	2MASS	P_{rot} (d)	Lit P_{rot} (d)	Ref. ^a	R_* (R_\odot)	M_* (M_\odot)	$v \sin i$ (km/s)	Ref. ^b	Inclination ($^\circ$)	Rvar
3664898 ^e	08294949 + 2646348	$0.46^{+1.12e-04}_{-1.12e-04}$	0.46	N16	$0.124^{+0.0037}_{-0.0037}$	0.1 ± 0.002	9.6 ± 1.5	R18	48.1 ± 10.9	$0.006^{+6.150e-05}_{-6.070e-05}$
13960751	00544803 + 2731035	$1.7^{+5.57e-03}_{-5.12e-03}$	1.70	N16	$0.282^{+0.0085}_{-0.0084}$	0.26 ± 0.006	9.0 ± 0.7	K18	80.6 ± 7.4	$0.006^{+8.350e-05}_{-8.510e-05}$
17970570 ^{c,d}	11224274 + 3755484	$0.56^{+4.08e-04}_{-4.03e-04}$	0.36	N16	$0.14^{+0.0042}_{-0.0042}$	0.11 ± 0.003	13.3 ± 0.8	K18	81.6 ± 6.5	$0.013^{+1.862e-04}_{-1.871e-04}$
53255031	05595569 + 5834155	$0.95^{+1.49e-03}_{-1.56e-03}$	0.95	N16	$0.254^{+0.0076}_{-0.0076}$	0.22 ± 0.005	9.2 ± 1.7	K18	47.2 ± 12.4	$0.004^{+3.530e-05}_{-3.510e-05}$
53307637	07464203 + 5726534	$0.82^{+1.03e-03}_{-1.01e-03}$	0.82	N16	$0.311^{+0.0093}_{-0.0093}$	0.29 ± 0.007	17.6 ± 0.8	K18	69.1 ± 7.6	$0.018^{+6.990e-05}_{-6.990e-05}$
58100576	00243478 + 3002295	$1.08^{+2.56e-03}_{-2.56e-03}$	1.08	N16	$0.26^{+0.0078}_{-0.0078}$	0.23 ± 0.006	13.0 ± 0.8	F18	81.9 ± 6.4	$0.01^{+7.110e-05}_{-7.080e-05}$
80859893 ^c	08012112 + 5624042	$0.12^{+1.18e-05}_{-1.15e-05}$	0.12	N16	$0.143^{+0.0042}_{-0.0042}$	0.11 ± 0.003	66.0 ± 0.5	K18	88.8 ± 1.1	$0.022^{+2.914e-04}_{-2.725e-04}$
84649454	04121693 + 6443560	$1.6^{+1.02e-02}_{-1.02e-02}$	1.59	N16	$0.221^{+0.0065}_{-0.0065}$	0.19 ± 0.004	7.2 ± 0.2	K18	84.7 ± 4.2	$0.003^{+3.620e-05}_{-3.450e-05}$
85334035 ^{c,e}	11115176 + 3332111	$7.74^{+1.15e-01}_{-1.10e-01}$	7.77	H11	$0.326^{+0.0098}_{-0.0098}$	0.31 ± 0.007	4.6 ± 0.7	F18	78.9 ± 9.7	$0.019^{+3.410e-05}_{-3.420e-05}$
88099283 ^c	09535523 + 2056460	$0.61^{+7.48e-04}_{-7.62e-04}$	0.62	N16	$0.179^{+0.0053}_{-0.0053}$	0.15 ± 0.003	10.1 ± 0.6	K18	43.8 ± 3.3	$0.003^{+4.100e-05}_{-3.870e-05}$
155113423	23025250 + 4338157	$0.35^{+4.73e-04}_{-4.72e-04}$	0.35	H11	$0.219^{+0.0065}_{-0.0065}$	0.19 ± 0.004	29.0 ± 1.5	K18	67.9 ± 8.0	$0.008^{+6.080e-05}_{-5.820e-05}$
156491690 ^{c,e}	14311348 + 7526423	$0.63^{+1.08e-04}_{-1.10e-04}$	0.63	N16	$0.199^{+0.006}_{-0.006}$	0.17 ± 0.004	14.3 ± 0.4	K18	64.5 ± 3.5	$0.006^{+3.960e-05}_{-4.100e-05}$
17300446 ^c	10030191 + 3433197	$0.86^{+8.24e-04}_{-8.27e-04}$	0.86	N16	$0.303^{+0.009}_{-0.009}$	0.28 ± 0.007	11.9 ± 0.2	K18	41.8 ± 0.9	$0.013^{+7.010e-05}_{-7.160e-05}$
178947176 ^{c,e}	04353618 - 2527347	$2.77^{+5.06e-02}_{-6.05e-02}$	2.78	K12	$0.403^{+0.0122}_{-0.0122}$	0.4 ± 0.01	7.1 ± 1.0	F18	72.4 ± 11.8	$0.003^{+2.210e-05}_{-2.330e-05}$
187092382 ^c	03571999 + 4107426	$0.57^{+6.32e-04}_{-5.32e-04}$	0.57	N16	$0.135^{+0.004}_{-0.004}$	0.11 ± 0.003	6.5 ± 0.8	K18	33.5 ± 4.6	$0.014^{+1.896e-04}_{-1.877e-04}$
219463771	13533877 + 7737083	$1.23^{+5.78e-03}_{-5.33e-03}$	1.23	N16	$0.29^{+0.0087}_{-0.0087}$	0.26 ± 0.006	8.9 ± 1.5	R18	53.8 ± 13.5	$0.008^{+3.110e-05}_{-3.110e-05}$
229614158	18315610 + 7730367	$0.86^{+3.26e-04}_{-3.33e-04}$	0.86	N16	$0.268^{+0.008}_{-0.008}$	0.24 ± 0.006	15.8 ± 0.7	F18	81.2 ± 6.3	$0.007^{+7.000e-05}_{-6.850e-05}$
233068870	18021660 + 6415445	$0.28^{+3.20e-05}_{-3.32e-05}$	0.28	N16	$0.195^{+0.0058}_{-0.0058}$	0.16 ± 0.004	10.3 ± 1.5	R18	17.4 ± 2.5	$0.003^{+2.400e-05}_{-2.480e-05}$
252110114	01015952 + 5410577	$0.28^{+8.81e-05}_{-8.92e-05}$	0.28	N16	$0.165^{+0.0049}_{-0.0049}$	0.13 ± 0.003	31.9 ± 3.1	R18	79.0 ± 8.5	$0.005^{+8.360e-05}_{-8.340e-05}$
266744225 ^c	07444018 + 0333089	$2.77^{+2.45e-02}_{-2.48e-02}$	2.80	A98	$0.333^{+0.0099}_{-0.0099}$	0.32 ± 0.007	4.0 ± 1.5	R18	53.2 ± 18.5	$0.007^{+1.700e-05}_{-1.620e-05}$
273589987	19510930 + 4628598	$0.59^{+1.34e-03}_{-1.17e-03}$	0.59	H11	$0.269^{+0.0079}_{-0.0079}$	0.24 ± 0.006	22.9 ± 2.3	R18	76.6 ± 9.7	$0.007^{+4.030e-05}_{-4.390e-05}$
283410775	22011310 + 2818248	$0.45^{+1.68e-04}_{-1.82e-04}$	0.45	M08	$0.313^{+0.0094}_{-0.0094}$	0.29 ± 0.007	35.4 ± 3.5	R18	76.5 ± 9.5	$0.011^{+4.000e-05}_{-3.860e-05}$
283866910 ^e	04171852 + 0849220	$0.37^{+1.99e-04}_{-2.05e-04}$	0.37	M22	$0.271^{+0.0082}_{-0.0081}$	0.24 ± 0.006	37.3 ± 1.1	K18	83.3 ± 4.9	$0.01^{+4.020e-05}_{-4.270e-05}$
286899254	15040626 + 4858538	$1.02^{+2.79e-03}_{-2.88e-03}$	1.02	H11	$0.327^{+0.0098}_{-0.0098}$	0.31 ± 0.007	11.3 ± 2.0	F18	48.8 ± 12.6	$0.014^{+1.527e-04}_{-1.575e-04}$
289972535	07555396 + 8323049	$1.11^{+1.15e-03}_{-1.18e-03}$	1.11	N16	$0.274^{+0.0083}_{-0.0083}$	0.25 ± 0.006	13.4 ± 1.5	R18	78.0 ± 9.2	$0.019^{+4.550e-05}_{-4.440e-05}$
291689873	23545147 + 3831363	$4.75^{+3.33e-02}_{-3.43e-02}$	4.76	K13	$0.316^{+0.0095}_{-0.0094}$	0.3 ± 0.007	3.6 ± 1.5	R18	66.8 ± 17.8	$0.026^{+5.900e-05}_{-6.350e-05}$
307913606	09245082 + 3041373	$0.37^{+5.30e-05}_{-5.18e-05}$	0.37	N16	$0.421^{+0.0125}_{-0.0125}$	0.42 ± 0.01	44.9 ± 3.1	K18	52.9 ± 5.6	$0.027^{+6.720e-05}_{-6.160e-05}$
309850275	15163731 + 5355457	$0.52^{+2.65e-04}_{-2.30e-04}$	0.52	N16	$0.202^{+0.0061}_{-0.0061}$	0.17 ± 0.004	19.2 ± 0.4	K18	81.6 ± 4.9	$0.014^{+1.372e-04}_{-1.357e-04}$
415508270 ^e	05041476 + 1103238	$0.84^{+2.29e-03}_{-2.11e-03}$	0.84	N16	$0.19^{+0.0058}_{-0.0059}$	0.16 ± 0.004	10.8 ± 1.4	K18	72.0 ± 11.5	$0.003^{+2.600e-05}_{-2.730e-05}$
440559522	06073185 + 4712266	$0.86^{+3.06e-03}_{-2.92e-03}$	0.86	N16	$0.356^{+0.0107}_{-0.0107}$	0.34 ± 0.008	20.8 ± 0.8	K18	81.0 ± 6.1	$0.013^{+6.930e-05}_{-7.090e-05}$

Table 1 continued

Table 1 (*continued*)

TID	2MASS	P_{rot} (d)	Lit P_{rot} (d)	Ref. ^a	R_* (R_\odot)	M_* (M_\odot)	$v \sin i$ (km/s)	Ref. ^b	Inclination ($^\circ$)	Rvar
-----	-------	---------------	-------------------	-------------------	---------------------	---------------------	-------------------	-------------------	--------------------------	------

NOTE— ^a Reference for literature periods: A98: [Alekseev & Bondar’ \(1998\)](#), M08: [Morin et al. \(2008\)](#), H11: [Hartman et al. \(2011\)](#), K12: [Kiraga \(2012\)](#), K13: [Kiraga & Stępień \(2013\)](#), N16: [Newton et al. \(2016b\)](#), and M22: [Medina et al. \(2022a\)](#). ^b Reference for $v \sin i$: F18: [Fouqué et al. \(2018\)](#), R18: [Reiners et al. \(2018\)](#), and K18: [Kesseli et al. \(2018\)](#). ^c Needed manual flare removal on the edges after stella. ^d Needed jitter term toggled on. ^e Needed both the jitter and the trend term toggled on. A portion of the machine-readable table, which includes additional columns such as mean $H\alpha$ EWs, mean $L_{H\alpha}/L_{bol}$, Spectral type, RUWE, TESS Contamination Ratio, TESS magnitude, apparent K magnitude, parallax, parallax error and Month observed.

2.3.2. Stellar Mass

Using M_K as a proxy for luminosity, we derive the masses of our targets following Mann et al. (2019). This relation applies to M dwarfs $0.075 < M/M_\odot < 0.70$ which encapsulate all of our targets. We use the corresponding Python package, `M_-M_K-2`, to calculate posterior probability distributions of mass for all 30 stars. We take the median of the distribution as our mass value, and compute the error as the 68% confidence interval.

2.3.3. Inclination

The $v \sin i$ of a star is determined from the rotational broadening of the spectral lines. To accurately determine the $v \sin i$, we require high resolution spectra with $R = (\Delta\lambda/\lambda) \sim 20,000 - 40,000$ (Newton et al. 2016b). We use $v \sin i$ from the literature (Fouqué et al. 2018; Reiners et al. 2018; Kesseli et al. 2018) along with our P_{rot} and R_* values to determine the inclination and its error for each target.

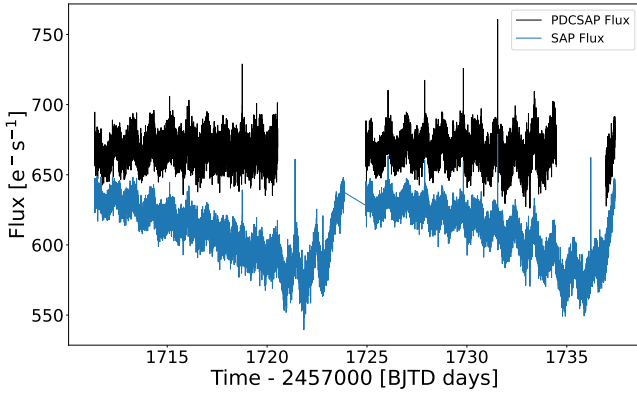


Figure 1. A `lightcurve` time-series comparing SAP flux and PDCSAP flux for TIC 343268431 (TESS magnitude 13.1). Long term systematic trends are seen from ~ 1710 to ~ 1722 Barycentric TESS Julian Date (BTJD - 2457000), the SAP flux decreases almost linearly and then increases after ~ 1722 . We also see that the pattern repeats in the second observation cycle. Meanwhile, the PDCSAP flux remains constant aside from the rotation modulations.

We use `inclinationmcmc`³ to calculate inclinations according to the framework from Masuda & Winn (2020). The code calculates a posterior probability distribution for $\cos i$, where i is the inclination. We then transform to i assuming that $0 < i < 90$ deg. We adopt the median value as the best-fit i and calculate error as the 68% confidence interval.

3. OBSERVATIONS AND DATA REDUCTION

3.1. Optical Photometric Data

TESS data products include 30-minute cadence full frame images and 2-minute cadence ‘postage stamp’ images of selected stars ($\sim 200,000$; Ricker et al. 2015). The Science Processing Operations Center produces 2-minute cadence light curves FITS files which are then released to the public via Mikulski Archive for Space Telescopes (MAST) archive (Jenkins et al. 2016). We use the 2-minute cadence light curves.

Within each light curve file there are two different measurements of flux: the Simple Aperture Photometry flux (SAP) and the Pre-search Data Conditioned Simple Aperture Photometry (PDCSAP). SAP sums the photon counts of a stellar source and subtracts from it the photon counts of the sky background. SAP also removes cosmic rays and “Argabrightening” events⁴ (Witteborn et al. 2011; Jenkins 2020). PDCSAP is derived from the SAP light curve, and accounts for systematics resulting from the spacecraft and its instruments, such as momentum dumps (Stumpe et al. 2012; Smith et al. 2012; Stumpe et al. 2014; Thompson et al. 2016). Example SAP and PDCSAP light curves are shown in Figure 1.

PDCSAP flux is effective at removing long-term trends. Newton et al. (2022) find that PDCSAP could also effect the observed rotation signature in some sectors; comparison of the SAP and PDCSAP light curves for stars in our sample indicates this is not a concern for us. Thus, for this paper we use the PDCSAP flux.

We use `lightcurve` (Lightcurve Collaboration et al. 2018; Barentsen et al. 2020) to download the TESS data. We use the quality bit-mask set to `default`, which removes bad cadences with major quality issues.

We select TESS data taken within a sector or 27 days of the date of our spectroscopic observing runs. For example, our 2019 October observing run corresponds to TESS sectors 16 and 17 (2019 September 11 - 2019 October 07 and 2019 October 07 - 2019 November 02, respectively). If targets were not observed by TESS in either of these two sectors, we considered neighboring sectors such as sector 18 (2019 November 02 - 2019 November 27). We examine long R_{var} in §4.1.3 and have notice minute changes in R_{var} for neighboring sectors. For observations that encompass multiple sectors, we apply `lightcurve`’s `stitch` method to stitch multiple sectors into a single light curve. Similar ranges are also use for the other observation runs and can be found in Table 2.

² https://github.com/awmann/M_-M_K-

³ <https://github.com/avanderburg/inclinationmcmc>

⁴ non-systematic diffused light of unknown origins that affects the background and the source apertures

Table 2. Observations

Month	Range of Observation (UTC)	Range of Observation (JD)	TESS Sectors	Total Objects*	Spectra per Target
2019 October	2458762.664754 – 2458767.595015	2019/10/06 – 2019/10/11	15 – 17	11	1
2020 January	2458851.833316 – 2458856.002801	2020/01/03 – 2020/01/07	19 & 20	9	3
2020 February	2458880.911557 – 2458895.841905	2020/02/01 – 2020/02/16	21 & 22	9	2 – 4
2020 December	2459188.724752 – 2459197.900665	2020/12/05 – 2020/12/14	32	4	25 – 135
2021 January	2459222.855154 – 2459222.8949	2021/01/08 – 2021/01/08	33	1	68

NOTE—*Note: There are 30 M dwarfs in total, but 3 of them were also observed a second time and 1 is the binary mentioned in Figure 7.

3.2. Optical Spectroscopic Data

We observe $H\alpha$ emission using OSMOS (Martini et al. 2011), mounted on the 2.4m Hiltner telescope at MDM Observatory in Arizona. Our setup consists of the blue VPH grism with a inner 1.2" slit and a 4x1k region of interest. The resulting spectra span 390-680 nm, with peak efficiency around 640 nm and a $R \sim 1600$ resolution. In this configuration, OSMOS is well-suited to single-object spectroscopy, particularly for our study of H-alpha emission at around 656.21 nm.

Our spectroscopic observations took place during 5 queue runs between 2019 October and 2021 January (Table 2). In total, we have 14 nights of data from OSMOS with the number of spectra increasing per observation cycle. For instance in 2019 October, we have 1 spectrum per star while in 2020 December we have more than 24 spectra per object. While a more specific account of the number of spectra can be found in the machine readable version of Table 1. The V magnitude of our stars vary from 17.47 to 11.19, which correlates to exposure times from 90s to 1200 seconds, respectively.

We use the `osmosreduct` pipeline provided by John Thorstensen⁵. With this semi-automated process, we perform standard flatfielding, bias subtraction, and wavelength calibration. We hand-check each file's aperture and remove bad points from the fit spectrum before extracting the 1D spectrum.

For the wavelength calibration, we use a master wavelength calibration which was created using a median-combination of an HgNe + Ne lamp and a Xe lamp. We wavelength-bin the data by comparing the wavelengths of known emission features to their observed wavelengths in each file. We linearly fit the residuals and find the corresponding scale factor and zero point of the data. We use these two factors to adjust the mas-

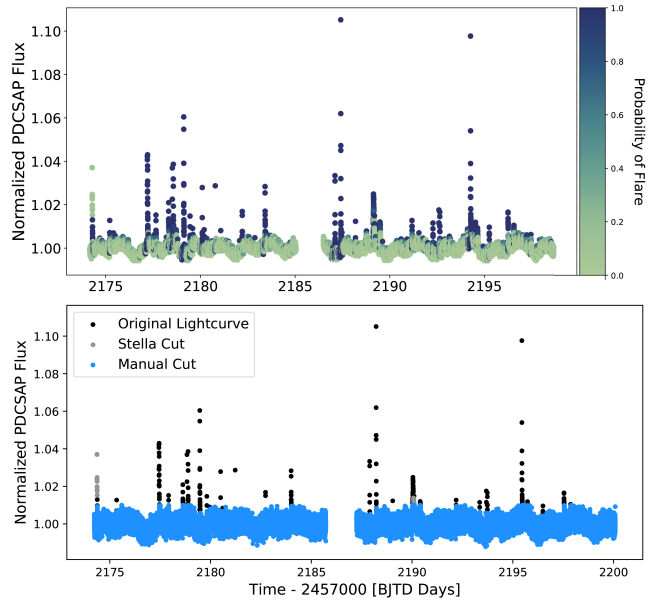


Figure 2. Normalized PDCSAP Flux vs. TESS Barycentric Julian Date (BJTD - 2457000). Top: The color bar represents the probability that each data point represents a flare, as determined by `stella`. The probabilities range from 0 to 1, where one constitutes a flare. While most large flares were removed, the one in the beginning of this observation was only reduced in strength, so that the large flare around 2175 d needed to be removed manually. All of the stars in the sample have more than one visible flare, while a handful have many flares such as this one. Bottom: Two of the flare removal methods discussed in §4.1. This bottom plot was created for all of the stars in our sample and is available as supplemental material.

ter and subsequently bin the data. We anchor the fit to lines at 404.7, 435.8, 546.1, and 640.2 nm by-hand; the rest are fit automatically using a polynomial of order 6.

The full spectra reduction amounts to for 63 objects with spectra range from 1-135 (Table 2). TESS cuts, as discussed above, reduce our target list to 30 stars.

⁵ <https://github.com/jrthorstensen/thorosmos>

4.1. Light Curve Analysis

We download *TESS* PDCSAP data using `lightkurve` for sectors coincident with our ground-based observations, and one sector before/after. As every star in our sample has at least one visible flare in the light curve, we first remove the flares (§4.1.1). We then fit the rotation modulation (§4.1.2) and calculate the semi-amplitude (§4.1.3).

4.1.1. Flare Removal

We use `stella`, a python package including a Convolutional Neural Network (CNN; Feinstein et al. 2020b) that has been trained to identify flares. We utilize 100 `stella` models trained on 2-min *TESS* data to detect the flares. Some models detect certain features better than others, so a combination of models yields more robust flare detections.

The ensemble of models gives a score between 0 and 1 at each data point, where 0 is a non-flare and 1 is a flare. Although it is not a probability, a comparison of visually-identified flares and the score shows that its an acceptable estimator of a flare. We identify that anything with a score above 0.5 as a flare; this value was chosen based on visual inspection of light curve plots. This value is also used in Feinstein et al. (2020b).

Some of the visual inspections show a few large flares that are missed by `stella` (Figure 2). Most of those flares are located in the beginning or end of the observation, or are lower energy but still apparent by eye. These may artificially elevate the semi-amplitude; thus, for 9 M dwarfs (flagged in Table 1), some features were removed manually by trimming the corresponding time stamps.

Further outlier rejection is performed as part of our stellar rotation fitting, which is effective at removing the remaining flares or distorted flares.

4.1.2. Gaussian Processes Fitting

Prior to fitting for stellar variability, we bin the data from 2 minute cadence to 10 minutes using `lightkurve`'s `bin` function to increase computational efficiency. Rotational variability is on timescales of hours so this is not expected to impact our modeling.

A sinusoidal model is not always effective at modeling the rotational variability of M dwarfs, which can be quasi-periodic and non-sinusoidal. For this reason, we use Gaussian processes to fit the rotational variability (e.g., Angus et al. 2018). We modify the `starspot` package to analyze the light curves (Angus 2021; Angus & Garcia Soto 2023)⁶. The Gaussian process kernel

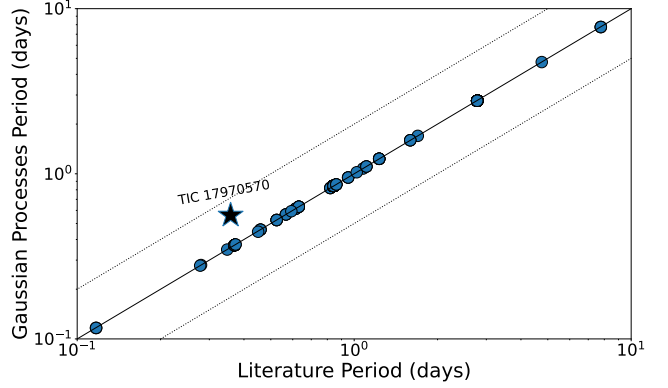


Figure 3. A comparison between the periods we find from `starspot` and rotation periods in the literature. The black star symbol denotes TIC 17970570, where our period is not quite double the period from Newton et al. (2016b). Re-analysis of data from MEarth shows that $P_{\text{rot}} = 0.5593 \pm 0.0004$ d is the true period, consistent with the result from *TESS*. We are therefore confident in our P_{rot} values for all 30 of our targets.

function is composed of two stochastically-driven simple harmonic oscillators, which indicate the primary (the rotation period, P_{rot}) and secondary ($P_{\text{rot}}/2$) modes.

Additional terms describe the amplitudes of variability, and how damped the two oscillators are. To account for other variability in the light curve, we can optionally include a jitter term that defines the white noise in the data and a trend term that accounts for long-term data unrelated to star spots. These two terms were only included when the code initially failed to converge on the correct period; otherwise, they have little effect on the fitting. We fit for jitter and/or long-term trends in 7 light curves (flagged in Table 1).

Some of our uniform priors are uninformative. Once we are satisfied that we have selected the correct period of the star, we place a truncated normal prior of 30% on $\log P_{\text{rot}}$ centered on the fiducial period of the star. This prevents unnecessary exploration of parameter space near $P_{\text{rot}}/2$.

First, we perform a maximum a posteriori (MAP) fit using `starspot`, then create a prediction of the stellar rotation model. Then we calculate the residuals of the MAP prediction by subtracting the model from the data. Data is kept when the absolute value of the residual is smaller than 4 times the root-mean-square (rms) of the residuals. This code is run a total of three times, rejecting outliers after each iteration.

Lastly, we sample the posterior of the stellar rotation model using the `PyMC3` package within our modified version of `starspot` (Salvatier et al. 2016). `starspot` uses a Markov Chain Monte Carlo (MCMC) to find the best fit parameters.

⁶ <https://github.com/agarciasoto18/starrotate>

As detailed in Table 1 and Figure 3, the periods of 29 M dwarfs match well with the literature. However, for one M dwarf TIC 17970570 (star symbol), *starspot* flagged a different period, of 0.5593 ± 0.0004 d. This is 1.6 times the literature value (0.358 d; Newton et al. 2016b). However, re-analysis of the data from MEarth’s Data Release 11 (2011-2012; Berta et al. 2012) data agrees with the period of 0.559 days, and we identify the 0.358 d signal as a 1 day alias. Thus, we can confirm the rotation periods for all 30 M dwarfs.

4.1.3. Semi-Amplitude using R_{var} Method

The R_{var} method of calculating the photometric amplitude was first defined by Basri et al. (2010, 2011) and modified by McQuillan et al. (2012, 2013). We calculate R_{var} by computing the difference between the 5th and 95th percentile of the median-normalized flux. R_{var} uncertainties are calculated using a simple Monte Carlo method, in which we re-draw new flux values at random using a normal distribution centered on the original flux values with width set by the flux errors. We then calculate R_{var} from the new fluxes. We perform 5000 iterations and pick the final R_{var} to be the 50th percentile, with the uncertainties from the 16th and 84th percentiles.

We examine R_{var} to set our definition of contemporaneous spectroscopic and photometric data, as we only have truly simultaneous observations for 18 out of our 30 objects. We pick stars in our sample with 5 or more sectors of TESS data, calculate R_{var} for each sector, and plot the R_{var} over time. In Figure 4, we show these plots for the two stars in our sample with the most TESS data: TIC 233068870 and TIC 229614158. For TIC 233068870, we remove one of the sectors from Figure 4 due systematic trends/non-stellar variability, which produces an artificially large value for R_{var} in that sector. Generally, R_{var} for both stars remains constant for 2-3 sectors, but it seems that the morphology can remain relatively consistent up around 6 sectors. It’s worth noting how R_{var} for both stars changes from one year to the next. This is also seen in Robertson et al. (2020). For example, TIC 233068870 increases from $R_{var} \lesssim 0.0035$ to $R_{var} \sim 0.0045$ in the span of a year. Given the result, we use TESS data taken within one to two sectors of the observation date of our spectroscopic data.

Finally, it is important to consider that R_{var} is sensitive to instrumental noise which has similar strengths to stellar variability, as with TIC 233068870 above. This would also mean toggling the long-term trend in *starspot* might also affect the R_{var} measurement. Although the R_{var} method is more robust than fitting for

the amplitude, the addition of noise increases the value of R_{var} (Basri et al. 2013; Johnson et al. 2021).

4.2. Spectral Analysis

4.2.1. Calculating $H\alpha$ Equivalent Widths

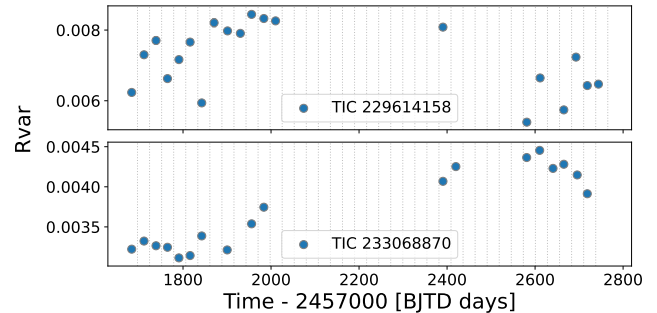


Figure 4. Two graphs of semi amplitude- R_{var} plotted over time. Top: TIC 229614158 and Bottom: TIC 233068870. The vertical lines represent the length of a TESS sector, approximately every 27.4 days.

To calculate $H\alpha$ Equivalent Widths (EWs), we first shift the spectra to rest wavelengths. To determine the velocity offset, we fit the $H\alpha$ lines in the M dwarf spectra with Gaussian distributions using *astropy’s specutils* (Astropy Collaboration et al. 2013; Collaboration 2018; Earl et al. 2019).

We use the standard definition of EW, following West et al. (2011) and Newton et al. (2017) and summing partial pixels assuming they are uniformly illuminated.

$$EW = \sum \left(1 - \frac{F(\lambda)}{F_c} \right) \delta\lambda, \quad (2)$$

where $F(\lambda)$ is the flux, $\delta\lambda$ is the pixel size, and F_c is the mean flux of the $H\alpha$ continuum level regions 6500-6550 Å and 6575-6625 Å. The summation is over width of the $H\alpha$ line, which is defined to be 8 Å (6558.8 - 6566.8 Å). We report $H\alpha$ EWs as negative values for emission.

4.2.2. Removing the Basal $H\alpha$ Contribution

Following the methodology in Newton et al. (2017) we remove the absorption component of the $H\alpha$ emission line. In M dwarfs with relatively little chromospheric heating, the $H\alpha$ line is in absorption. As chromospheric heating increases the absorption line strength increases, reaching a maximum positive EW of ~ 0.7 Å. To evaluate only the emission component, we must therefore define and account for the base absorption level at a given mass. As in Newton et al. (2017), our spectral resolution is too low to distinguish between strengthening absorption or emission for a weakly active star. Thus, we only set the base emission level.

Newton et al. (2017) showed that as mass decreases, the maximum $H\alpha$ absorption EWs also decreases. We define a basal absorption value (EW_{basal}), and subtract it from the measured value ($EW_{measured}$, from Equation 2) to calculate the final relative value (EW).

$$EW_{basal} = -5.36570831 + 7.62481452 M - 2.88931216 M^2 + 0.52686116 M^3 \quad (3)$$

$$EW = EW_{measured} - EW_{basal} \quad (4)$$

where M is the stellar mass in M_{\odot} . We use these relative EWs for all further calculations including $L_{H\alpha}/L_{bol}$.

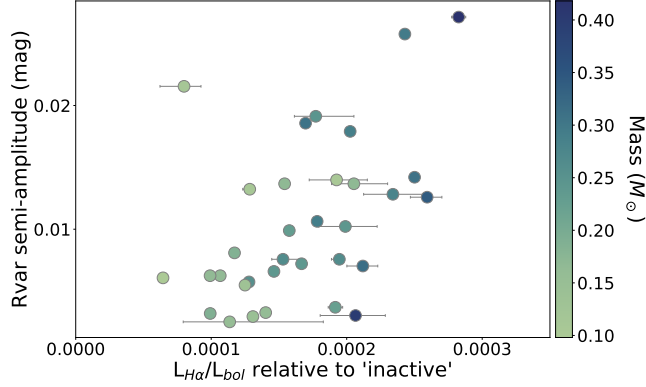


Figure 5. Semi amplitude, R_{var} plotted against the $H\alpha$ strength, $L_{H\alpha}/L_{bol}$. The x-axis error bars for the OSMOS data in this case represent the range in $L_{H\alpha}/L_{bol}$. There is a possible correlation between R_{var} and $L_{H\alpha}/L_{bol}$, with more active stars showing higher photometric variability.

We then normalize by the bolometric luminosity of the star to get $L_{H\alpha}/L_{bol}$. In practice, to calculate $L_{H\alpha}/L_{bol}$, we multiply EW by the χ factor. This allows us to calculate $L_{H\alpha}/L_{bol}$ without absolute flux calibrated data (Walkowicz et al. 2004). The χ factor is determined from the division of the spectral continuum flux (the mean flux between 6550-6560 and 6570-6580 Å) by the apparent bolometric flux for stars with flux-calibrated data. The χ factor is calibrated using stellar models, then is calculated from color indices. We adopt the χ values from Newton et al. (2017), which are derived following Douglas et al. (2014).

5. RESULTS

5.1. $H\alpha$ Activity vs Amplitude Relation

Newton et al. (2017) find that stars with greater $H\alpha$ activity have more photometric variability. As in that work, we plot the $L_{H\alpha}/L_{bol}$ and amplitude (or in our case, R_{var} ; Figure 5). Note that the $L_{H\alpha}/L_{bol}$ error bars correspond to the range in $L_{H\alpha}/L_{bol}$ values due to multiple spectroscopic observations. For example, the star

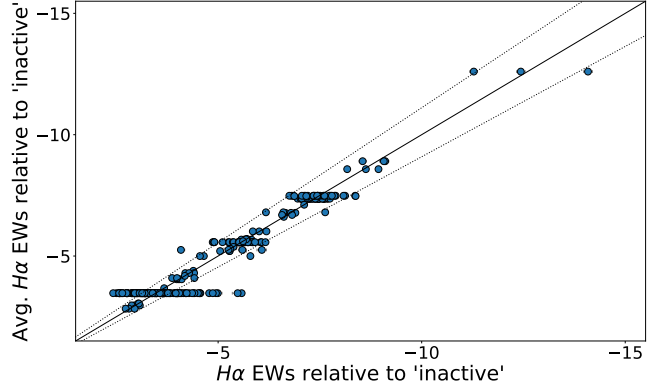


Figure 6. The comparison of the average relative $H\alpha$ EWs for each M Dwarf against their range of relative $H\alpha$ EWs. The dotted lines represent 10% variation from the mean value. TIC 415508270 has the largest range: 30.2% to 60.8% variation from the mean value.

with the largest range, TIC 415508270, has 135 measurements. In other words, some of these stars have $H\alpha$ emission variability (see §5.2).

We find a tentative positive correlation between $L_{H\alpha}/L_{bol}$ and R_{var} . The Spearman rank correlation (ρ) tests for a correlation between variables. Similar to how we extract the R_{var} and its errors, we run a simple Monte Carlo methods program to randomize the ρ and the p -values and set the low and high error bars to the 16th and 84th percentile. We calculate a $\rho = 0.479^{+0.155}_{-0.169}$ with $p = 0.005^{+0.075}_{-0.005}$. This falls between 0 (poor correlation) and 1 (positive monotonic correlation), so we consider it a moderate positive correlation. Conversely, given the large error in p -value, we cannot say that this result is not by chance. In contrast, Newton et al. (2017) find evidence for a correlation with $\rho = 0.39 \pm 0.03$ and $p = 4 \times 10^{-8}$; further analysis is warranted.

Figure 5 also shows the mass dependence of the relative $L_{H\alpha}/L_{bol}$ (Newton et al. 2017). As the stellar mass increases, relative $L_{H\alpha}/L_{bol}$ also increases. We get $\rho = 0.755^{+0.084}_{-0.115}$ with $p = (0.01^{+1.39}_{-0.01}) \times 10^{-4}$, meaning that the mass is positively correlated to relative $L_{H\alpha}/L_{bol}$.

This is consistent with other studies, which find a decrease in $L_{H\alpha}/L_{bol}$ for late-type M dwarfs ($< M4$ or $M6$; e.g., Gizis et al. 2002; West et al. 2004; Lee et al. 2010; Kruse et al. 2010; Bell et al. 2012; Zhang et al. 2023). This mass dependence is also seen in both the saturated and unsaturated regime with $\log R'_{HK}$ (Schrijver & Rutten 1987; Rauscher & Marcy 2006; Houdebine et al. 2017; Boudreaux et al. 2022), but no such variation is seen in X-rays (Wright & Drake 2016). Finally, there is a mass-dependence in the saturated magnetic field strength for M dwarfs (Vidotto et al. 2014),

which could perhaps explain the variations in $H\alpha$ activity. This suggests that the magnetic field may be affecting the chromosphere differently than the corona.

We conclude that contemporaneous spectroscopy and photometry, and a more uniform and flexible method of measuring semi-amplitudes, overall does not result in a clearer amplitude-activity relation. However, our data suggest that there may be a positive correlation between photometric semi-amplitude and $H\alpha$ emission in M dwarfs which is also observed in other spectra types (Zhang et al. 2023).

5.2. $H\alpha$ Variability

Here we investigate the variability of $H\alpha$ EWs for stars in our sample with multiple observations. Figure 6 compares the average $H\alpha$ EWs to all $H\alpha$ EWs measured for that star. All stars with multiple spectra show some short term $H\alpha$ variability. Excluding stars with a single spectrum (11 stars), 7/19 stars show variability above 10% of the mean. However, it is important to note that 16 stars in this subset have less than 4 spectra. The stars with more than 25 spectra, excluding a binary plotted in Figure 7, all show short-term variability. This result does not seem likely to be caused by sampling bias, but we need follow-up observations to confirm.

Next, we search for simultaneous $H\alpha$ and photometric variations. Flares can enhance $H\alpha$ emission, and Medina et al. (2022a) showed that length of time for a flare are around 20-45 minutes which aligns with some $H\alpha$ variability timescales. Thus, in Figure Figure 7, we plot the TESS light curve on top and the $H\alpha$ EWs measurements on the bottom to see if $H\alpha$ emission variability can be attributed to flaring. Both our photometric and spectroscopic data sets align in time for three out of four objects observed on December 2020. All three show $H\alpha$ EWs varying on timescales of less than an hour, similar to (Medina et al. 2022a).

TIC 220044948 (left) is an M2 star with $P_{rot} = 0.6$ days—it has a RUWE ~ 2 so it was not included in the overall sample. On the first night of observations, it shows $H\alpha$ emission enhancement corresponding to a flare observed in TESS—around 0.01 on the x-axis. However there are several peaks following that event, which could suggest that $H\alpha$ emission is from stochastic flaring. Alternative explanations for the variability include low energy flares below the capabilities of TESS (Medina et al. 2022a), or contribution of a binary companion.

On the other hand, TIC 415508270 (middle) is not a binary. It is a fully convective M5 with a $P_{rot} = 0.84$ days. Like, TIC 220044948, it shows multiple $H\alpha$ EW peaks on its second night of observation. The rough time between each peak for TIC 220044948 and TIC

415508270 both happen on the order of 20-45 minutes. Although, in this case there isn't clear flare enhancement in the light curve. There are no clear flares in the light curve that align with the large $H\alpha$ peaks.

Lastly, TIC 178947176 (right) is a fully convective M3.5 with $P_{rot} = 2.77$ days. It shows a single peak in the first night. Unlike the other two stars, this star does not have consecutive peaks so we cannot give it a rough timing estimate.

Overall, we see flare-induced enhancement in $H\alpha$ EW for one star, but the driving factor for other $H\alpha$ variability is still unclear. Another possibility is that the variability not tied to a flare or binary companion could be intrinsic in nature. Nevertheless, a more in depth analysis for these stars and a larger sample will be the subject of a future paper.

6. DISCUSSION: POSSIBLE ORIGINS OF SCATTER IN THE AMPLITUDE-ACTIVITY RELATION

Like Newton et al. (2017), we find a positive relationship between $L_{H\alpha}/L_{bol}$ and variability amplitude. Newton et al. (2017) find $\rho_{H\alpha} = 0.39 \pm 0.03$ with $p = 4 \times 10^{-8}$, while we find $\rho_{H\alpha} = 0.479^{+0.155}_{-0.169}$. However, we find only weak evidence against the null hypothesis ($p = 0.005^{+0.075}_{-0.005}$) and we cannot confirm if this correlation is due to random chance at this time. There is no indication that contemporaneous observations or more robust amplitude measurements decrease the scatter in this relationship. Hence, the scatter in $H\alpha$ emission might be an intrinsic property of M dwarfs, unrelated to their overall spot coverage. Below, we consider possible explanations for our results.

6.1. Inclination of the stellar rotation axis

On the Sun, and possibly some other solar-like stars, spot groups appear where the magnetic field rises through the stellar surface, and migrate towards the equator as a cycle progresses (Vogt et al. 1999; Strassmeier & Bartus 2000). While for fast rotating cool dwarfs, it is theorized that the spots groups appear at poles due to the greater strength of the Coriolis force over the buoyancy force (Schuessler & Solanki 1992). Thus, many permutations of stellar inclination and spot latitude can produce the same photometric amplitudes (Basri & Shah 2020). This is because R_{var} is not tracing the spot coverage but rather the hemispheric spot distribution asymmetry, thus R_{var} is also susceptible to spot evolution (e.g., Luger et al. 2019; Basri & Shah 2020; Luger et al. 2021). Moreover, low-amplitude variability could indicate large pole-on/polar spots that are almost always in view (Berdyugina et al. 2002; Berdyug-

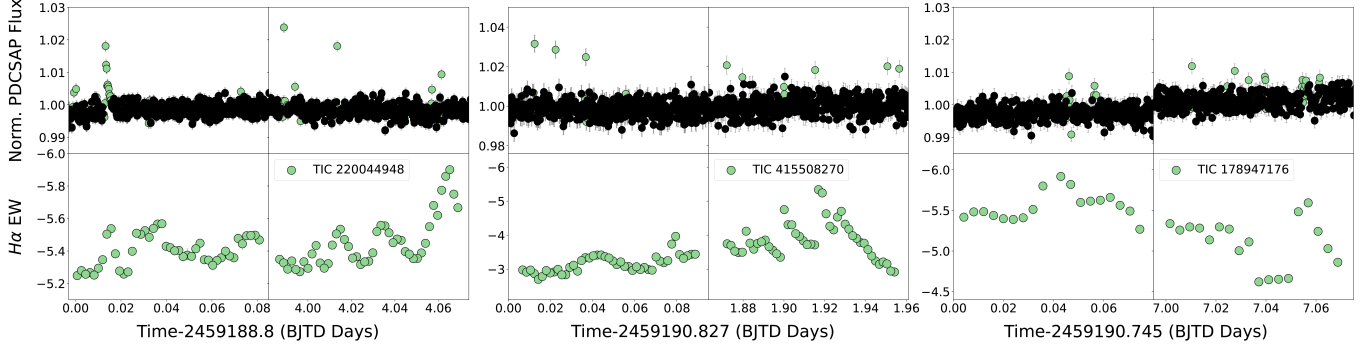


Figure 7. The original PDCSAP light curve on the top, $H\alpha$ EWs in the middle, and number of σ_{std} from the mean $H\alpha$ EWs in the bottom against time. Left: 2 nights for TIC 220044948, Middle: 2 nights for TIC 415508270, Right: 2 nights for TIC 178947176. The light green circles are the raw light curve and the black circles is the light curve after *stella* removed the flares. For the middle and bottom panel, the light green circles are each target-specific $H\alpha$ EW observation.

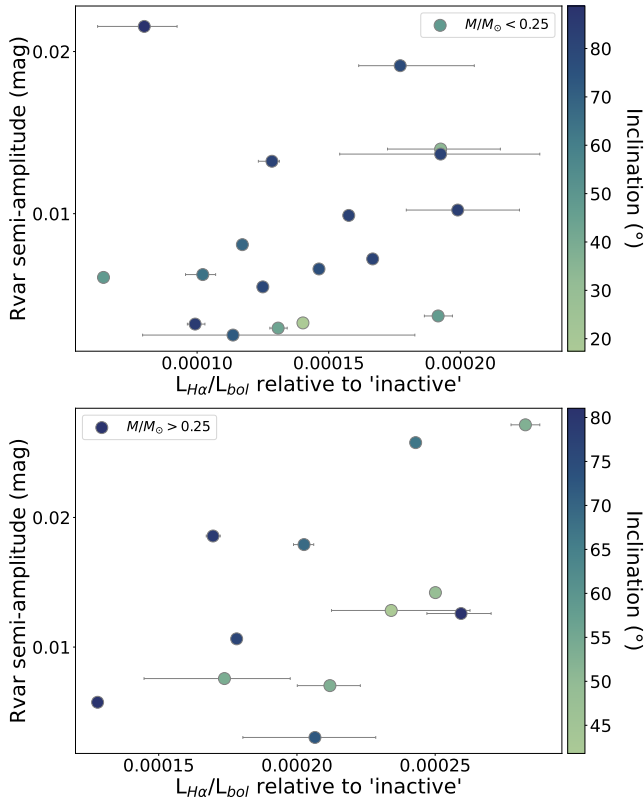


Figure 8. Same set up as Figure 5, except the color bar is inclination. Top: Stars with mass $< 0.25 M_{\odot}$. Bottom: Stars with mass $> 0.25 M_{\odot}$, separated as detailed in [Newton et al. \(2016b\)](#). The “error bars” in this case represent the full range in $H\alpha$ luminosity measurements. Inclination does not visibly correlate with $L_{H\alpha}/L_{bol}$ but there might some indication in the low-mass bin that smaller R_{var} have smaller inclinations.

ina 2005; Rackham et al. 2019; Luger et al. 2021), but could also be due to small spots in an equator-on view.

However, we find no correlation with inclination (Figure 8). The Spearman rank correlation coefficients for both mass bins are not consistent with a correlation

and the p -value indicates that it’s likely due to random errors. For masses, $< 0.25 M_{\odot}$, $\rho_i = 0.365^{+0.230}_{-0.261}$, $p = 0.135^{+0.458}_{-0.126}$, while for Mass $> 0.25 M_{\odot}$: $\rho_i = -0.175^{+0.315}_{-0.266}$ and $p = 0.457^{+0.372}_{-0.332}$. We would expect that smaller R_{var} would correspond to smaller inclinations (pole-on). While, the relationship between the lower mass bin and the inclination show a very weak positive correlation, accounting for the error bars, the p -values are large.

This lack of observed correlation may be due to our small sample size and lack of pole-on rotators. For instance, in Table 1, we see the lowest inclination to be 17.43 ± 2.53 , while the highest is 88.95 ± 0.93 (equator-on). The majority (20/30) fall on the higher end of inclinations ($\gtrsim 65^\circ$) thus we are lacking pole-on stars which might drive a more significant correlation. Given these limitations, for our small sample of 30 M dwarfs, we cannot confirm if inclinations have a correlation with photometric amplitude.

6.2. Activity and photometric variability as tracers of underlying stellar surface

The scatter between $L_{H\alpha}/L_{bol}$ and R_{var} seems to be intrinsic. One possibility for the scatter is our choice of proxy for starspots: photometric amplitude. Amplitudes encode multiple degenerate spot properties such as spot distribution, coverage, temperature and size. In addition, we are ignoring contribution from bright spots such as plages and faculae. Albeit to a lesser extent, these bright regions can also impact the photometry (Jackson & Jeffries 2012, 2013; Rackham et al. 2018, 2019; Johnson et al. 2021).

Although $H\alpha$ is the primary activity indicator for M dwarfs, several solar studies use Ca II H&K ($\log R'_{HK}$) as an chromospheric activity indicator (e.g., Karoff et al. 2016; Mandal et al. 2017; Morris et al. 2018, 2019). We therefore test whether we observe any correlation between R_{var} and $\log R'_{HK}$ (Figure 9).

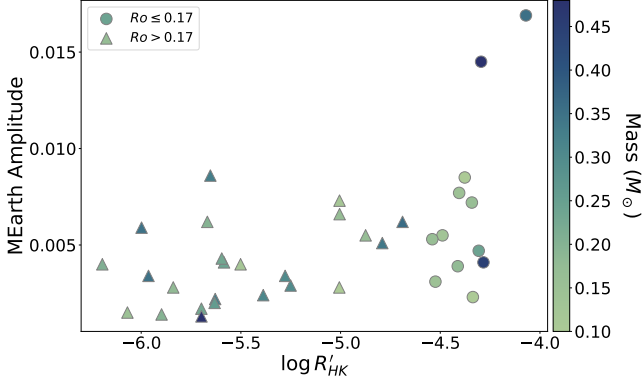


Figure 9. This plot is the MEarth fitted-amplitude plotted against the $\log R'_{HK}$ (RUWE < 1.6) using data from Boudreaux et al. (2022). In order to compare to our sample, we differentiate stars in the unsaturated regime (triangles) and stars in the saturated regime (circles). The stars in the saturated regime are defined as stars with Rossby < 0.17 ± 0.04 .

We apply the selection criteria from our sample, including RUWE < 1.6, to the Ca II H&K sample in Boudreaux et al. (2022). An affect of our choice in instrument is the location of our stars in the saturated regime, thus we also cut by the critical Rossby number < 0.17 ± 0.04 listed in the paper. The relationship between amplitude and $\log(R'_{HK})$ for stars in the saturated regime (circles) is $\rho_{HK} = 0.348^{+0.285}_{-0.334}$, $p = 0.246^{+0.457}_{-0.219}$, a weakly positive correlation that could be due to chance. Conversely, if we include stars in the unsaturated regime (triangles), or stars with periods longer than around 15 days, we get $\rho_{HK} = 0.498^{+0.132}_{-0.154}$ and $p_{HK} = 0.002^{+0.038}_{-0.002}$ or a statistically significant positive relationship. We propose that including unsaturated stars may make the correlation clear enough to improve p -value as well. If this is the case, our $H\alpha$ results may also hinge on the inclusion of unsaturated stars.

Finally, while $H\alpha$ and Ca II H&K are both tracers for plagues, photometric amplitude traces starspots. There have been multiple studies that show that small plagues can be co-located with spots (e.g., Radick et al. 1998, 2018; Järvinen et al. 2007, 2008; Morris et al. 2018; Fang et al. 2020). Mandal et al. (2017) compared plagues and spots on the sun and found that on longer timescales, such as the 11 year solar-cycle, these two features are very correlated. On shorter timescales such as days and months, however, they are not correlated due to the shorter lifetime of spots. Preminger & Walton (2007) find a similar result for faculae and spots. While, we try to account for spot evolution by using contemporaneous data, it is therefore possible that spots and plagues are not well-correlated in M dwarfs, or that our results are

affected by the degeneracies in spot properties derived from photometric amplitudes.

6.3. $H\alpha$ Short-term Variability

Lastly, a third possibility could be the short-term variability of $H\alpha$. Previous works have demonstrated significant short-timescale variability of $H\alpha$ (e.g., Kruse et al. 2010; Lee et al. 2010; Medina et al. 2022a; Duvvuri et al. 2023) and Ca II H&K (e.g., Suárez Mascareño et al. 2016; Kumar & Fares 2023; Duvvuri et al. 2023). For example, Kruse et al. (2010) shows that 74% of their M dwarf sample (with $H\alpha$ emission and independent of spectral type) vary between 15 minutes to an hour while Medina et al. (2022a) finds variability within 20-45 minutes. We also find short term variation within that range with $H\alpha$ EWs peaks increasing 1-3 σ_{std} over the mean value.

The dominant source for the short-term variability might be low-energy flares (e.g., Liebert et al. 2003; Lee et al. 2010; Hilton 2011; Medina et al. 2020, 2022a; Zhang et al. 2023; Duvvuri et al. 2023). A flare occurs when a magnetic field loop breaks: part of it snaps off and releases energy while the other part reconnects at a lower energy state. Some of that released energy heats the chromosphere and enhances $H\alpha$ emission (Cram & Mullan 1979; Medina et al. 2020, 2022a).

Medina et al. (2020) show fully convective M dwarfs show an activity-flare rate relation similar to the saturated rotation-activity relation: the logarithmic flaring rate per day decreases sharply when $H\alpha$ emission decreases below a critical value ($H\alpha$ EW < -0.71\AA). Interestingly, they find that in the “saturated” regime, the flare rate shallowly increases with increasing emission (< -0.71\AA) in the saturated regime. This could explain the flaring activity described in §4.1.1. Although the authors note it was unclear if the individual EWs are enhanced by flares, Medina et al. (2022a) compare the timescales of low-energy flare decay to the $H\alpha$ emission variability and find them to be similar.

Moreover, Maehara et al. (2021) look at contemporaneous photometric data and $H\alpha$ spectra for YZ CMi (TIC 266744225, amplitude $\sim 3.6\%$ in the TESS band). Previous inclination measurements places it between 36^{+17}_{-14} (Baroch et al. 2020) and 60 degrees (Morin et al. 2008), which matches our results of 60 ± 18 . During a epoch of low flaring activity, they find that large $H\alpha$ emission corresponded to dips in rotational modulation. However, for an epoch with high flaring activity there was no significant modulation in $H\alpha$ EW. The believe that the difference could be due a difference in inclination and spot latitudes. This would suggest the short-term variability in $H\alpha$ is due to flaring from newly

emerging small active regions, in agreement with Medina et al. (2022a).

Hence, the dominate source of $H\alpha$ enhancement for these stars of high activity seems to be the low-energy flares rather than the active regions on the star. As we saw in §5.2, TIC 220044948 shows clear $H\alpha$ enhancement during its first night of observation similar to the one seen in Medina et al. (2022a). Alternatively, we also see similar peaks and a larger $H\alpha$ peak during the second night that do not align with large flares in TESS—also true for the second night of TIC 415508270. Given the rough periodicity of the peaks, between 20–45 minutes, we believe these could be due to low energy flares that are below the sensibility of TESS detection. We also noticed only 7/19 stars with variability greater than 10% of the $H\alpha$ EW mean. These stars all have more than one spectrum, but only 3 M dwarfs with more than 25 spectra. Thus, we would need more time-resolved $H\alpha$ spectra in order to match more flares with the optical photometry.

7. SUMMARY

We expand on the work of Newton et al. (2017) by obtaining contemporaneous $H\alpha$ spectroscopy and photometric data from TESS. Our goal is to tighten the relationship between photometric variability and $H\alpha$ emission. However, we find no significant change in the relationship between photometric amplitude and $L_{H\alpha}/L_{bol}$. We suggest scatter is not explained by the lack of simultaneity, stellar mass, or inclination. Other sources of scatter must dominate such as low-energy flares.

Consistent with previous works, we saw that the photometric variability amplitude could remain constant for multiple months. In contrast, we saw that $H\alpha$ emission varies on shorter timescales than rotation. Medina et al. (2022a) suggest that small flares are the dominate source of these short-term fluctuations corresponding to flare decays of 20–45 minutes. However, this does not mean spots do not also contribute. Further research into spot properties and activity in M dwarfs will elucidate the connection between these phenomena and the diversity amongst M dwarfs.

As we saw with the Spearman correlation coefficient and the p -value for Ca II H&K and amplitude relationship, when we included the stars in the unsaturated regime the relationship strengthened. Thus, it is pos-

sible that if we include stars the unsaturated regime, we could get a smaller p -value and a stronger overall relationship. However, the large p -value for both $H\alpha$ luminosity and Ca II H&K with photometric amplitude measurements could be due attributed to small number statistics. It is possible that a larger sample of high-activity stars could identify a clearer trend.

1 We are really grateful to proxy observer Justin Ru-
2 pert for taking the spectroscopic data. We also
3 thank John R. Thorstensen, Burçin Mutlu-Pakdil, Brian
4 C. Chaboyer, Thomas M. Boudreaux, Keighley E.
5 Rockcliffe, Rayna Rampalli, Andrew Vanderburg and
6 Kathryn E. Weil for their contributions, advice and con-
7 versations that improved the manuscript.

8 This work has made use of data from the Euro-
9 pean Space Agency (ESA) mission *Gaia* (<https://www.cosmos.esa.int/gaia>), processed by the *Gaia* Data Pro-
10 cessing and Analysis Consortium (DPAC, <https://www.cosmos.esa.int/web/gaia/dpac/consortium>). Funding
11 for the DPAC has been provided by national institu-
12 tions, in particular the institutions participating in the
13 *Gaia* Multilateral Agreement. This paper includes data
14 collected by the *TESS* mission. Funding for the *TESS*
15 mission is provided by the NASA’s Science Mission Di-
16 rectorate.
17
18

Facilities: MDM:Hiltner (Martini et al. 2011), TESS (Ricker et al. 2015)

Software: *astropy* (Astropy Collaboration et al. 2013; Collaboration 2018), *celerite2* (Foreman-Mackey et al. 2017, 2020b), *edmc* (Vanderburg 2021), *ernlib* (<https://github.com/ernewton/ernlib>), *exoplanet* (Foreman-Mackey et al. 2020a; Agol et al. 2020), *inclinationmcmc* (<https://github.com/avanderburg/inclinationmcmc>), *IRAF* (Tody 1986, 1993; National Optical Astronomy Observatories 1999), *lightcurve* (Lightcurve Collaboration et al. 2018; Barentsen et al. 2020), *M-M-K* (<https://github.com/awmann/M-M-K>; Mann et al. 2019), *NumPy* (Oliphant 2006), *PyMC3* (Salvatier et al. 2016), *readmultispec* (Gullikson 2014), *SciPy* (Virtanen et al. 2020), *specutils* (Earl et al. 2019), *starspot* (Angus 2021), *stella* (Feinstein et al. 2020a), *thorosmos* (<https://github.com/jrthorstensen/thorosmos>), *thorsky* (<https://github.com/jrthorstensen/thorsky>)

REFERENCES

- Agol, E., Luger, R., & Foreman-Mackey, D. 2020, The Astronomical Journal, 159, 123, doi: 10.3847/1538-3881/ab4fee
- Alekseev, I. Y., & Bondar’, N. I. 1998, Astronomy Reports, 42, 655. <https://ui.adsabs.harvard.edu/abs/1998ARep...42..655A>

- Angus, R. 2021, Zenodo, doi: [10.5281/zenodo.4613887](https://doi.org/10.5281/zenodo.4613887)
- Angus, R., & Garcia Soto, A. 2023, *agarciasoto18/starrotate*: Alternate starrotate for paper, Zenodo, doi: [10.5281/zenodo.7697238](https://doi.org/10.5281/zenodo.7697238)
- Angus, R., Morton, T., Aigrain, S., Foreman-Mackey, D., & Rajpaul, V. 2018, *Monthly Notices of the Royal Astronomical Society*, 474, 2094, doi: [10.1093/mnras/stx2109](https://doi.org/10.1093/mnras/stx2109)
- Astropy Collaboration, Robitaille, T. P., Tollerud, E. J., et al. 2013, *Astronomy and Astrophysics*, 558, A33, doi: [10.1051/0004-6361/201322068](https://doi.org/10.1051/0004-6361/201322068)
- Barentsen, G., Hedges, C., Vinícius, Z., et al. 2020, *KeplerGO/lightkurve*: Lightkurve v1.11.0, Zenodo, doi: [10.5281/zenodo.3836658](https://doi.org/10.5281/zenodo.3836658)
- Baroch, D., Morales, J. C., Ribas, I., et al. 2020, *Astronomy & Astrophysics*, Volume 641, id.A69, 12 pp., 641, A69, doi: [10.1051/0004-6361/202038213](https://doi.org/10.1051/0004-6361/202038213)
- Basri, G., & Shah, R. 2020, *The Astrophysical Journal*, 901, 14, doi: [10.3847/1538-4357/abae5d](https://doi.org/10.3847/1538-4357/abae5d)
- Basri, G., Walkowicz, L. M., & Reiners, A. 2013, *The Astrophysical Journal*, 769, 37, doi: [10.1088/0004-637X/769/1/37](https://doi.org/10.1088/0004-637X/769/1/37)
- Basri, G., Walkowicz, L. M., Batalha, N., et al. 2010, *The Astrophysical Journal Letters*, 713, L155, doi: [10.1088/2041-8205/713/2/L155](https://doi.org/10.1088/2041-8205/713/2/L155)
- . 2011, *The Astronomical Journal*, 141, 20, doi: [10.1088/0004-6256/141/1/20](https://doi.org/10.1088/0004-6256/141/1/20)
- Bell, K. J., Hilton, E. J., Davenport, J. R. A., et al. 2012, *Publications of the Astronomical Society of the Pacific*, 124, 14, doi: [10.1086/664024](https://doi.org/10.1086/664024)
- Berdyugina, S. V. 2005, *Living Reviews in Solar Physics*, 2, 8, doi: [10.12942/lrsp-2005-8](https://doi.org/10.12942/lrsp-2005-8)
- Berdyugina, S. V., Pelt, J., & Tuominen, I. 2002, *Astronomy and Astrophysics*, 394, 505, doi: [10.1051/0004-6361:20021179](https://doi.org/10.1051/0004-6361:20021179)
- Berta, Z. K., Irwin, J., Charbonneau, D., Burke, C. J., & Falco, E. E. 2012, *The Astronomical Journal*, 144, 145, doi: [10.1088/0004-6256/144/5/145](https://doi.org/10.1088/0004-6256/144/5/145)
- Boisse, I., Bouchy, F., Hébrard, G., et al. 2011, *Astronomy & Astrophysics*, 528, A4, doi: [10.1051/0004-6361/201014354](https://doi.org/10.1051/0004-6361/201014354)
- Boudreaux, T. M., Newton, E. R., Mondrik, N., Charbonneau, D., & Irwin, J. 2022, *The Astrophysical Journal*, 929, 80, doi: [10.3847/1538-4357/ac5cbf](https://doi.org/10.3847/1538-4357/ac5cbf)
- Browning, M. K., Basri, G., Marcy, G. W., West, A. A., & Zhang, J. 2010, *The Astronomical Journal*, 139, 504, doi: [10.1088/0004-6256/139/2/504](https://doi.org/10.1088/0004-6256/139/2/504)
- Bryson, S., Kunimoto, M., Kopparapu, R. K., et al. 2021, *The Astronomical Journal*, 161, 36, doi: [10.3847/1538-3881/abc418](https://doi.org/10.3847/1538-3881/abc418)
- Cameron, R. H., Dikpati, M., & Brandenburg, A. 2017, *Space Science Reviews*, 210, 367, doi: [10.1007/s11214-015-0230-3](https://doi.org/10.1007/s11214-015-0230-3)
- Chabrier, G., & Baraffe, I. 1997, *Astronomy and Astrophysics*, 327, 1039, <http://adsabs.harvard.edu/abs/1997A%26A...327.1039C>
- Charbonneau, P. 2010, *Living Reviews in Solar Physics*, 7, 3, doi: [10.12942/lrsp-2010-3](https://doi.org/10.12942/lrsp-2010-3)
- Collaboration, T. A. 2018, *astropy v3.0.4*: a core python package for astronomy, Zenodo, doi: [10.5281/zenodo.1461593](https://doi.org/10.5281/zenodo.1461593)
- Cooke, B. F., Pollacco, D., West, R., McCormac, J., & Wheatley, P. J. 2018, *Astronomy & Astrophysics*, 619, A175, doi: [10.1051/0004-6361/201834014](https://doi.org/10.1051/0004-6361/201834014)
- Cortés-Contreras, M., Béjar, V. J. S., Caballero, J. A., et al. 2017, *Astronomy & Astrophysics*, Volume 597, id.A47, 13 pp., 597, A47, doi: [10.1051/0004-6361/201629056](https://doi.org/10.1051/0004-6361/201629056)
- Cram, L. E., & Mullan, D. J. 1979, *The Astrophysical Journal*, 234, 579, doi: [10.1086/157532](https://doi.org/10.1086/157532)
- Davenport, J. R. A. 2016, *The Astrophysical Journal*, 829, 23, doi: [10.3847/0004-637X/829/1/23](https://doi.org/10.3847/0004-637X/829/1/23)
- Delfosse, X., Forveille, T., Perrier, C., & Mayor, M. 1998, *Astronomy and Astrophysics*, 331, 581, <http://adsabs.harvard.edu/abs/1998A%26A...331..581D>
- Donati, J.-F., Morin, J., Petit, P., et al. 2008, *Monthly Notices of the Royal Astronomical Society*, 390, 545, doi: [10.1111/j.1365-2966.2008.13799.x](https://doi.org/10.1111/j.1365-2966.2008.13799.x)
- Douglas, S. T., Agüeros, M. A., Covey, K. R., et al. 2014, *The Astrophysical Journal*, 795, 161, doi: [10.1088/0004-637X/795/2/161](https://doi.org/10.1088/0004-637X/795/2/161)
- Duvvuri, G. M., Pineda, J. S., Berta-Thompson, Z. K., France, K., & Youngblood, A. 2023, *The Astronomical Journal*, 165, 12, doi: [10.3847/1538-3881/ac9b49](https://doi.org/10.3847/1538-3881/ac9b49)
- Earl, N., Jones, C., Kerzendorf, W., et al. 2019, *astropy/specutils*: v0.6, Zenodo, doi: [10.5281/zenodo.3450769](https://doi.org/10.5281/zenodo.3450769)
- Fang, X.-S., Bidin, C. M., Zhao, G., Zhang, L.-Y., & Bharat Kumar, Y. 2020, *Monthly Notices of the Royal Astronomical Society*, 495, 2949, doi: [10.1093/mnras/staa1392](https://doi.org/10.1093/mnras/staa1392)
- Feiden, G. A., & Chaboyer, B. 2012, *The Astrophysical Journal*, 757, 42, doi: [10.1088/0004-637X/757/1/42](https://doi.org/10.1088/0004-637X/757/1/42)
- Feinstein, A., Montet, B., & Ansdell, M. 2020a, *The Journal of Open Source Software*, 5, 2347, doi: [10.21105/joss.02347](https://doi.org/10.21105/joss.02347)
- Feinstein, A. D., Montet, B. T., Ansdell, M., et al. 2020b, *The Astronomical Journal*, 160, 219, doi: [10.3847/1538-3881/abac0a](https://doi.org/10.3847/1538-3881/abac0a)

- Foreman-Mackey, D., Agol, E., Ambikasaran, S., & Angus, R. 2017, *Astrophysics Source Code Library*, ascl:1709.008, <http://adsabs.harvard.edu/abs/2017ascl.soft09008F>
- Foreman-Mackey, D., Luger, R., Czekala, I., et al. 2020a, *exoplanet-dev/exoplanet: exoplanet v0.3.2*, Zenodo, doi: [10.5281/zenodo.3785072](https://doi.org/10.5281/zenodo.3785072)
- Foreman-Mackey, D., Agol, E., Angus, R., et al. 2020b, *dfm/celerite: celerite v0.4.0*, Zenodo, doi: [10.5281/zenodo.3934421](https://doi.org/10.5281/zenodo.3934421)
- Fouqué, P., Moutou, C., Malo, L., et al. 2018, *Monthly Notices of the Royal Astronomical Society*, 475, 1960, doi: [10.1093/mnras/stx3246](https://doi.org/10.1093/mnras/stx3246)
- Gaia Collaboration, G., Prusti, T., de Bruijne, J. H. J., et al. 2016, *Astronomy and Astrophysics*, 595, A1, doi: [10.1051/0004-6361/201629272](https://doi.org/10.1051/0004-6361/201629272)
- Gaia Collaboration, G., Brown, A. G. A., Vallenari, A., et al. 2018, *Astronomy and Astrophysics*, 616, A1, doi: [10.1051/0004-6361/201833051](https://doi.org/10.1051/0004-6361/201833051)
- Gaia Collaboration, G., Vallenari, A., Brown, A. G. A., et al. 2022, *arXiv e-prints*. <https://ui.adsabs.harvard.edu/abs/2022arXiv220800211G>
- Gizis, J. E., Reid, I. N., & Hawley, S. L. 2002, *The Astronomical Journal*, 123, 3356, doi: [10.1086/340465](https://doi.org/10.1086/340465)
- Gullikson, K. 2014, *General-Scripts_v1.0*, Zenodo, doi: [10.5281/zenodo.10013](https://doi.org/10.5281/zenodo.10013)
- Hartman, J. D., Bakos, G. Á., Noyes, R. W., et al. 2011, *The Astronomical Journal*, 141, 166, doi: [10.1088/0004-6256/141/5/166](https://doi.org/10.1088/0004-6256/141/5/166)
- Haywood, R. D., Collier Cameron, A., Queloz, D., et al. 2014, *Monthly Notices of the Royal Astronomical Society*, 443, 2517, doi: [10.1093/mnras/stu1320](https://doi.org/10.1093/mnras/stu1320)
- Henry, T. J., Jao, W.-C., Subasavage, J. P., et al. 2006, *The Astronomical Journal*, 132, 2360, doi: [10.1086/508233](https://doi.org/10.1086/508233)
- Hilton, E. J. 2011, PhD thesis, University of Washington. <https://ui.adsabs.harvard.edu/abs/2011PhDT.....144H>
- Houdebine, E. R., Mullan, D. J., Bercu, B., Paletou, F., & Gebran, M. 2017, *The Astrophysical Journal*, 837, 96, doi: [10.3847/1538-4357/aa5cad](https://doi.org/10.3847/1538-4357/aa5cad)
- Jackson, R. J., & Jeffries, R. D. 2012, *Monthly Notices of the Royal Astronomical Society*, 423, 2966, doi: [10.1111/j.1365-2966.2012.21119.x](https://doi.org/10.1111/j.1365-2966.2012.21119.x)
- . 2013, *Monthly Notices of the Royal Astronomical Society*, 431, 1883, doi: [10.1093/mnras/stt304](https://doi.org/10.1093/mnras/stt304)
- Jenkins, J. M. 2020, *Kepler Science Document*, KSCI-19081-003, Edited by Jon M. Jenkins., 19
- Jenkins, J. M., Twicken, J. D., McCauliff, S., et al. 2016, *Proceedings of the SPIE*, Volume 9913, id. 99133E 20 pp. (2016)., 9913, 99133E, doi: [10.1117/12.2233418](https://doi.org/10.1117/12.2233418)
- Johnson, L. J., Norris, C. M., Unruh, Y. C., et al. 2021, *Monthly Notices of the Royal Astronomical Society*, 504, 4751, doi: [10.1093/mnras/stab1190](https://doi.org/10.1093/mnras/stab1190)
- Järvinen, S. P., Berdyugina, S. V., Korhonen, H., Ilyin, I., & Tuominen, I. 2007, *Astronomy and Astrophysics*, 472, 887, doi: [10.1051/0004-6361:20077551](https://doi.org/10.1051/0004-6361:20077551)
- Järvinen, S. P., Korhonen, H., Berdyugina, S. V., et al. 2008, *Astronomy and Astrophysics*, 488, 1047, doi: [10.1051/0004-6361:200809837](https://doi.org/10.1051/0004-6361:200809837)
- Karoff, C., Knudsen, M. F., De Cat, P., et al. 2016, *Nature Communications*, 7, 11058, doi: [10.1038/ncomms11058](https://doi.org/10.1038/ncomms11058)
- Kesseli, A. Y., Muirhead, P. S., Mann, A. W., & Mace, G. 2018, *The Astronomical Journal*, 155, 225, doi: [10.3847/1538-3881/aabccb](https://doi.org/10.3847/1538-3881/aabccb)
- Kim, Y.-C., & Demarque, P. 1996, *The Astrophysical Journal*, 457, 340, doi: [10.1086/176733](https://doi.org/10.1086/176733)
- Kiraga, M. 2012, *Acta Astronomica*, 62, 67. <https://ui.adsabs.harvard.edu/abs/2012AcA....62...67K>
- Kiraga, M., & Stepień, K. 2013, *Acta Astronomica*, 63, 53. <https://ui.adsabs.harvard.edu/abs/2013AcA....63...53K>
- Kraus, A. L., Tucker, R. A., Thompson, M. I., Craine, E. R., & Hillenbrand, L. A. 2011, *The Astrophysical Journal*, 728, 48, doi: [10.1088/0004-637X/728/1/48](https://doi.org/10.1088/0004-637X/728/1/48)
- Kruse, E. A., Berger, E., Knapp, G. R., et al. 2010, *The Astrophysical Journal*, 722, 1352, doi: [10.1088/0004-637X/722/2/1352](https://doi.org/10.1088/0004-637X/722/2/1352)
- Kumar, M., & Fares, R. 2023, *Monthly Notices of the Royal Astronomical Society*, 518, 3147, doi: [10.1093/mnras/stac2766](https://doi.org/10.1093/mnras/stac2766)
- Lee, K.-G., Berger, E., & Knapp, G. R. 2010, *The Astrophysical Journal*, 708, 1482, doi: [10.1088/0004-637X/708/2/1482](https://doi.org/10.1088/0004-637X/708/2/1482)
- Lehtinen, J. J., Käpylä, M. J., Olsper, N., & Spada, F. 2021, *The Astrophysical Journal*, 910, 110, doi: [10.3847/1538-4357/abe621](https://doi.org/10.3847/1538-4357/abe621)
- Liebert, J., Kirkpatrick, J. D., Cruz, K. L., et al. 2003, *The Astronomical Journal*, 125, 343, doi: [10.1086/345514](https://doi.org/10.1086/345514)
- Lightkurve Collaboration, Cardoso, J. V. d. M., Hedges, C., et al. 2018, *Astrophysics Source Code Library*, ascl:1812.013. <http://adsabs.harvard.edu/abs/2018ascl.soft12013L>
- Lindgren, L. 2018, *Re-normalising the astrometric chi-square in Gaia DR2*, Tech. Note GAIA-C3-TN-LU-LL-124, Technical Note, Lund Observatory. http://www.rssd.esa.int/doc_fetch.php?id=3757412
- Lindgren, L., Klioner, S. A., Hernández, J., et al. 2021, *Astronomy and Astrophysics*, 649, A2, doi: [10.1051/0004-6361/202039709](https://doi.org/10.1051/0004-6361/202039709)

- Luger, R., Agol, E., Foreman-Mackey, D., et al. 2019, *The Astronomical Journal*, 157, 64, doi: [10.3847/1538-3881/aae8e5](https://doi.org/10.3847/1538-3881/aae8e5)
- Luger, R., Foreman-Mackey, D., Hedges, C., & Hogg, D. W. 2021, *The Astronomical Journal*, 162, 123, doi: [10.3847/1538-3881/abfdb8](https://doi.org/10.3847/1538-3881/abfdb8)
- Maehara, H., Notsu, Y., Namekata, K., et al. 2021, *Publications of the Astronomical Society of Japan*, 73, 44, doi: [10.1093/pasj/psaa098](https://doi.org/10.1093/pasj/psaa098)
- Magaudda, E., Stelzer, B., Covey, K. R., et al. 2020, *Astronomy & Astrophysics*, 638, A20, doi: [10.1051/0004-6361/201937408](https://doi.org/10.1051/0004-6361/201937408)
- Mamajek, E. E., & Hillenbrand, L. A. 2008, *The Astrophysical Journal*, 687, 1264, doi: [10.1086/591785](https://doi.org/10.1086/591785)
- Mandal, S., Chatterjee, S., & Banerjee, D. 2017, *The Astrophysical Journal*, 835, 158, doi: [10.3847/1538-4357/835/2/158](https://doi.org/10.3847/1538-4357/835/2/158)
- Mann, A. W., Feiden, G. A., Gaidos, E., Boyajian, T., & Braun, K. v. 2015, *The Astrophysical Journal*, 804, 64, doi: [10.1088/0004-637X/804/1/64](https://doi.org/10.1088/0004-637X/804/1/64)
- Mann, A. W., Dupuy, T., Kraus, A. L., et al. 2019, *The Astrophysical Journal*, 871, 63, doi: [10.3847/1538-4357/aaf3bc](https://doi.org/10.3847/1538-4357/aaf3bc)
- Manset, N., & Donati, J.-F. 2003, in *Polarimetry in Astronomy*, Vol. 4843 (International Society for Optics and Photonics), 425–436, doi: [10.1117/12.458230](https://doi.org/10.1117/12.458230)
- Martini, P., Stoll, R., Derwent, M. A., et al. 2011, *Publications of the Astronomical Society of the Pacific*, 123, 187, doi: [10.1086/658357](https://doi.org/10.1086/658357)
- Masuda, K., & Winn, J. N. 2020, *The Astronomical Journal*, 159, 81, doi: [10.3847/1538-3881/ab65be](https://doi.org/10.3847/1538-3881/ab65be)
- McQuillan, A., Aigrain, S., & Mazeh, T. 2013, *Monthly Notices of the Royal Astronomical Society*, 432, 1203, doi: [10.1093/mnras/stt536](https://doi.org/10.1093/mnras/stt536)
- McQuillan, A., Aigrain, S., & Roberts, S. 2012, *Astronomy and Astrophysics*, 539, A137, doi: [10.1051/0004-6361/201016148](https://doi.org/10.1051/0004-6361/201016148)
- Medina, A. A., Charbonneau, D., Winters, J. G., Irwin, J., & Mink, J. 2022a, *The Astrophysical Journal*, 928, 185, doi: [10.3847/1538-4357/ac5738](https://doi.org/10.3847/1538-4357/ac5738)
- Medina, A. A., Winters, J. G., Irwin, J. M., & Charbonneau, D. 2020, *The Astrophysical Journal*, 905, 107, doi: [10.3847/1538-4357/abc686](https://doi.org/10.3847/1538-4357/abc686)
- . 2022b, *The Astrophysical Journal*, 935, 104, doi: [10.3847/1538-4357/ac77f9](https://doi.org/10.3847/1538-4357/ac77f9)
- Mekkaden, M. V. 1985, *Astrophysics and Space Science*, 117, 381, doi: [10.1007/BF00650163](https://doi.org/10.1007/BF00650163)
- Middelkoop, F. 1981, *Astronomy & Astrophysics*, 101, 295. <http://adsabs.harvard.edu/abs/1981A%26A...101..295M>
- Mohanty, S., & Basri, G. 2003, *The Astrophysical Journal*, 583, 451, doi: [10.1086/345097](https://doi.org/10.1086/345097)
- Morin, J., Donati, J.-F., Petit, P., et al. 2010, *Monthly Notices of the Royal Astronomical Society*, 407, 2269, doi: [10.1111/j.1365-2966.2010.17101.x](https://doi.org/10.1111/j.1365-2966.2010.17101.x)
- Morin, J., Donati, J. F., Petit, P., et al. 2008, *Monthly Notices of the Royal Astronomical Society*, 390, 567, doi: [10.1111/j.1365-2966.2008.13809.x](https://doi.org/10.1111/j.1365-2966.2008.13809.x)
- Morrell, S., & Naylor, T. 2019, *Monthly Notices of the Royal Astronomical Society*, 489, 2615, doi: [10.1093/mnras/stz2242](https://doi.org/10.1093/mnras/stz2242)
- Morris, B. M., Curtis, J. L., Douglas, S. T., et al. 2018, *The Astronomical Journal*, 156, 203, doi: [10.3847/1538-3881/aae1ab](https://doi.org/10.3847/1538-3881/aae1ab)
- Morris, B. M., Curtis, J. L., Sakari, C., Hawley, S. L., & Agol, E. 2019, *The Astronomical Journal*, 158, 101, doi: [10.3847/1538-3881/ab2e04](https://doi.org/10.3847/1538-3881/ab2e04)
- National Optical Astronomy Observatories. 1999, *Astrophysics Source Code Library*, ascl:9911.002. <http://adsabs.harvard.edu/abs/1999ascl.soft11002N>
- Newton, E. R., Irwin, J., Charbonneau, D., et al. 2017, *The Astrophysical Journal*, 834, 85, doi: [10.3847/1538-4357/834/1/85](https://doi.org/10.3847/1538-4357/834/1/85)
- Newton, E. R., Irwin, J., Charbonneau, D., Berta-Thompson, Z. K., & Dittmann, J. A. 2016a, *The Astrophysical Journal*, 821, L19, doi: [10.3847/2041-8205/821/1/L19](https://doi.org/10.3847/2041-8205/821/1/L19)
- Newton, E. R., Irwin, J., Charbonneau, D., et al. 2016b, *The Astrophysical Journal*, 821, 93, doi: [10.3847/0004-637X/821/2/93](https://doi.org/10.3847/0004-637X/821/2/93)
- Newton, E. R., Rampalli, R., Kraus, A. L., et al. 2022, *The Astronomical Journal*, 164, 115, doi: [10.3847/1538-3881/ac8154](https://doi.org/10.3847/1538-3881/ac8154)
- Núñez, A., Agüeros, M. A., Covey, K. R., & López-Morales, M. 2017, in *Revista Mexicana de Astronomía y Astrofísica Conference Series*, Vol. 49, *Revista Mexicana de Astronomía y Astrofísica Conference Series*, 91–91. <https://ui.adsabs.harvard.edu/abs/2017RMxAC..49...91N>
- Oliphant, T. E. 2006, *A guide to NumPy*, Vol. 1 (Trelgol Publishing USA)
- Park, C., Jaffe, D. T., Yuk, I.-S., et al. 2014, *Proceedings of the SPIE*, Volume 9147, id. 91471D 12 pp. (2014)., 9147, 91471D, doi: [10.1117/12.2056431](https://doi.org/10.1117/12.2056431)
- Parker, E. N. 1955, *The Astrophysical Journal*, 122, 293, doi: [10.1086/146087](https://doi.org/10.1086/146087)
- Pont, F., Knutson, H., Gilliland, R. L., Moutou, C., & Charbonneau, D. 2008, *Monthly Notices of the Royal Astronomical Society*, 385, 109, doi: [10.1111/j.1365-2966.2008.12852.x](https://doi.org/10.1111/j.1365-2966.2008.12852.x)

- Preminger, D. G., & Walton, S. R. 2007, *Solar Physics*, 240, 17, doi: [10.1007/s11207-007-0335-2](https://doi.org/10.1007/s11207-007-0335-2)
- Quirrenbach, A., Amado, P. J., Seifert, W., et al. 2012, Ground-based and Airborne Instrumentation for Astronomy IV. Proceedings of the SPIE, Volume 8446, article id. 84460R, 13 pp. (2012)., 8446, 84460R, doi: [10.1117/12.925164](https://doi.org/10.1117/12.925164)
- Rackham, B. V., Apai, D., & Giampapa, M. S. 2018, *The Astrophysical Journal*, 853, 122, doi: [10.3847/1538-4357/aaa08c](https://doi.org/10.3847/1538-4357/aaa08c)
- . 2019, *The Astronomical Journal*, 157, 96, doi: [10.3847/1538-3881/aaf892](https://doi.org/10.3847/1538-3881/aaf892)
- Radick, R. R., Lockwood, G. W., Henry, G. W., Hall, J. C., & Pevtsov, A. A. 2018, *The Astrophysical Journal*, 855, 75, doi: [10.3847/1538-4357/aaae3](https://doi.org/10.3847/1538-4357/aaae3)
- Radick, R. R., Lockwood, G. W., Skiff, B. A., & Baliunas, S. L. 1998, *The Astrophysical Journal Supplement Series*, 118, 239, doi: [10.1086/313135](https://doi.org/10.1086/313135)
- Rampalli, R., Vanderburg, A., Bieryla, A., et al. 2019, *The Astronomical Journal*, 158, 62, doi: [10.3847/1538-3881/ab27c2](https://doi.org/10.3847/1538-3881/ab27c2)
- Rauscher, E., & Marcy, G. W. 2006, *\pasp*, 118, 617, doi: [10.1086/503021](https://doi.org/10.1086/503021)
- Rayner, J., Tokunaga, A., Jaffe, D., et al. 2016, Proceedings of the SPIE, Volume 9908, id. 990884 17 pp. (2016)., 9908, 990884, doi: [10.1117/12.2232064](https://doi.org/10.1117/12.2232064)
- Reiners, A., Basri, G., & Browning, M. 2009, *The Astrophysical Journal*, 692, 538, doi: [10.1088/0004-637X/692/1/538](https://doi.org/10.1088/0004-637X/692/1/538)
- Reiners, A., Joshi, N., & Goldman, B. 2012, *The Astronomical Journal*, 143, 93, doi: [10.1088/0004-6256/143/4/93](https://doi.org/10.1088/0004-6256/143/4/93)
- Reiners, A., Schüssler, M., & Passetger, V. M. 2014, *The Astrophysical Journal*, 794, 144, doi: [10.1088/0004-637X/794/2/144](https://doi.org/10.1088/0004-637X/794/2/144)
- Reiners, A., Zechmeister, M., Caballero, J. A., et al. 2018, *Astronomy and Astrophysics*, 612, A49, doi: [10.1051/0004-6361/201732054](https://doi.org/10.1051/0004-6361/201732054)
- Reiners, A., Shulyak, D., Käpylä, P. J., et al. 2022, *Astronomy and Astrophysics*, 662, A41, doi: [10.1051/0004-6361/202243251](https://doi.org/10.1051/0004-6361/202243251)
- Ricker, G. R., Winn, J. N., Vanderspek, R., et al. 2015, *Journal of Astronomical Telescopes, Instruments, and Systems*, 1, 014003, doi: [10.1117/1.JATIS.1.1.014003](https://doi.org/10.1117/1.JATIS.1.1.014003)
- Rizzuto, A. C., Vanderburg, A., Mann, A. W., et al. 2018, *The Astronomical Journal*, 156, 195, doi: [10.3847/1538-3881/aadf37](https://doi.org/10.3847/1538-3881/aadf37)
- Robertson, P., Stefansson, G., Mahadevan, S., et al. 2020, *The Astrophysical Journal*, 897, 125, doi: [10.3847/1538-4357/ab989f](https://doi.org/10.3847/1538-4357/ab989f)
- Robinson, Jr., R. D. 1980, *The Astrophysical Journal*, 239, 961, doi: [10.1086/158184](https://doi.org/10.1086/158184)
- Saar, S. H. 1988, *The Astrophysical Journal*, 324, 441, doi: [10.1086/165907](https://doi.org/10.1086/165907)
- Salvatier, J., Wiecki, T. V., & Fonnesbeck, C. 2016, *PeerJ Computer Science*, 2, e55, doi: [10.7717/peerj-cs.55](https://doi.org/10.7717/peerj-cs.55)
- Schrijver, C. J., & Rutten, R. G. M. 1987, *Astronomy and Astrophysics*, 177, 143. <https://ui.adsabs.harvard.edu/abs/1987A&A...177..143S/abstract>
- Schuessler, M., & Solanki, S. K. 1992, *Astronomy and Astrophysics*, 264, L13. <https://ui.adsabs.harvard.edu/abs/1992A&A...264L..13S/abstract>
- Shulyak, D., Reiners, A., Engeln, A., et al. 2017, *Nature Astronomy*, 1, 0184, doi: [10.1038/s41550-017-0184](https://doi.org/10.1038/s41550-017-0184)
- Shulyak, D., Reiners, A., Nagel, E., et al. 2019, *Astronomy and Astrophysics*, 626, A86, doi: [10.1051/0004-6361/201935315](https://doi.org/10.1051/0004-6361/201935315)
- Skrutskie, M. F., Cutri, R. M., Stiening, R., et al. 2006, *The Astronomical Journal*, 131, 1163, doi: [10.1086/498708](https://doi.org/10.1086/498708)
- Smith, J. C., Stumpe, M. C., Van Cleve, J. E., et al. 2012, *Publications of the Astronomical Society of the Pacific*, 124, 1000, doi: [10.1086/667697](https://doi.org/10.1086/667697)
- Spada, F., Demarque, P., Kim, Y. C., & Sills, A. 2013, *The Astrophysical Journal*, 776, 87, doi: [10.1088/0004-637X/776/2/87](https://doi.org/10.1088/0004-637X/776/2/87)
- Stassun, K. G., Oelkers, R. J., Pepper, J., et al. 2018, *The Astronomical Journal*, 156, 102, doi: [10.3847/1538-3881/aad050](https://doi.org/10.3847/1538-3881/aad050)
- Strassmeier, K. G., & Bartus, J. 2000, *Astronomy and Astrophysics*, 354, 537. <https://ui.adsabs.harvard.edu/abs/2000A&A...354..537S/abstract>
- Stumpe, M. C., Smith, J. C., Catanzarite, J. H., et al. 2014, *Publications of the Astronomical Society of the Pacific*, 126, 100, doi: [10.1086/674989](https://doi.org/10.1086/674989)
- Stumpe, M. C., Smith, J. C., Van Cleve, J. E., et al. 2012, *Publications of the Astronomical Society of the Pacific*, 124, 985, doi: [10.1086/667698](https://doi.org/10.1086/667698)
- Suárez Mascareño, A., Rebolo, R., & González Hernández, J. I. 2016, *Astronomy and Astrophysics*, 595, A12, doi: [10.1051/0004-6361/201628586](https://doi.org/10.1051/0004-6361/201628586)
- Thompson, S. E., Fraquelli, D., Van Cleve, J. E., & Caldwell, D. A. 2016, *Kepler Archive Manual*, KDMC-10008-006, 39
- Tody, D. 1986, IN: *Instrumentation in astronomy VI*; Proceedings of the Meeting, Tucson, AZ, Mar. 4-8, 1986. Part 2 (A87-36376 15-35). Bellingham, WA, Society of Photo-Optical Instrumentation Engineers, 1986, p. 733., 627, 733, doi: [10.1117/12.968154](https://doi.org/10.1117/12.968154)

- . 1993, *Astronomical Data Analysis Software and Systems II*, A.S.P. Conference Series, Vol. 52, 1993, R. J. Hanisch, R. J. V. Brissenden, and Jeannette Barnes, eds., p. 173., 52, 173.
<http://adsabs.harvard.edu/abs/1993ASPC...52..173T>
- Valenti, J. A., Marcy, G. W., & Basri, G. 1995, *The Astrophysical Journal*, 439, 939, doi: [10.1086/175231](https://doi.org/10.1086/175231)
- Vanderburg, A. 2021, Zenodo, doi: [10.5281/zenodo.5599854](https://doi.org/10.5281/zenodo.5599854)
- Vaughan, A. H. 1980, *Publications of the Astronomical Society of the Pacific*, 92, 392, doi: [10.1086/130684](https://doi.org/10.1086/130684)
- Vidotto, A. A., Gregory, S. G., Jardine, M., et al. 2014, *Monthly Notices of the Royal Astronomical Society*, 441, 2361, doi: [10.1093/mnras/stu728](https://doi.org/10.1093/mnras/stu728)
- Virtanen, P., Gommers, R., Oliphant, T. E., et al. 2020, *Nature Methods*, 17, 261, doi: [10.1038/s41592-019-0686-2](https://doi.org/10.1038/s41592-019-0686-2)
- Vogt, S. S., Hatzes, A. P., Misch, A. A., & Kürster, M. 1999, *The Astrophysical Journal Supplement Series*, 121, 547, doi: [10.1086/313195](https://doi.org/10.1086/313195)
- Wakeford, H. R., Lewis, N. K., Fowler, J., et al. 2019, *The Astronomical Journal*, 157, 11, doi: [10.3847/1538-3881/aaf04d](https://doi.org/10.3847/1538-3881/aaf04d)
- Walkowicz, L. M., Hawley, S. L., & West, A. A. 2004, *Publications of the Astronomical Society of the Pacific*, 116, 1105, doi: [10.1086/426792](https://doi.org/10.1086/426792)
- West, A. A., Hawley, S. L., Walkowicz, L. M., et al. 2004, *The Astronomical Journal*, 128, 426, doi: [10.1086/421364](https://doi.org/10.1086/421364)
- West, A. A., Morgan, D. P., Bochanski, J. J., et al. 2011, *The Astronomical Journal*, 141, 97, doi: [10.1088/0004-6256/141/3/97](https://doi.org/10.1088/0004-6256/141/3/97)
- Winters, J. G., Charbonneau, D., Henry, T. J., et al. 2021, *The Astronomical Journal*, 161, 63, doi: [10.3847/1538-3881/abcc74](https://doi.org/10.3847/1538-3881/abcc74)
- Winters, J. G., Henry, T. J., Jao, W.-C., et al. 2019, *The Astronomical Journal*, 157, 216, doi: [10.3847/1538-3881/ab05dc](https://doi.org/10.3847/1538-3881/ab05dc)
- Witteborn, F. C., Van Cleve, J., Borucki, W., Argabright, V., & Hascall, P. 2011, *Proceedings of the SPIE*, Volume 8151, id. 815117 (2011)., 8151, 815117, doi: [10.1117/12.892850](https://doi.org/10.1117/12.892850)
- Wright, N. J., & Drake, J. J. 2016, *Nature*, 535, 526, doi: [10.1038/nature18638](https://doi.org/10.1038/nature18638)
- Wright, N. J., Drake, J. J., Mamajek, E. E., & Henry, G. W. 2011, *The Astrophysical Journal*, 743, 48, doi: [10.1088/0004-637X/743/1/48](https://doi.org/10.1088/0004-637X/743/1/48)
- Wright, N. J., Newton, E. R., Williams, P. K. G., Drake, J. J., & Yadav, R. K. 2018, *Monthly Notices of the Royal Astronomical Society*, 479, 2351, doi: [10.1093/mnras/sty1670](https://doi.org/10.1093/mnras/sty1670)
- Zhang, L.-y., Su, T., Misra, P., et al. 2023, *The Astrophysical Journal Supplement Series*, 264, 17, doi: [10.3847/1538-4365/ac9b28](https://doi.org/10.3847/1538-4365/ac9b28)
- Zhang, Z., Zhou, Y., Rackham, B. V., & Apai, D. 2018, *The Astronomical Journal*, 156, 178, doi: [10.3847/1538-3881/aade4f](https://doi.org/10.3847/1538-3881/aade4f)